

IMPROVED LABORATORY TRANSITION PROBABILITIES FOR Er II AND
APPLICATION TO THE ERBIUM ABUNDANCES OF THE SUN AND FIVE r -PROCESS
RICH, METAL-POOR STARS

(short title: Er II Transition Probabilities and Abundances)

J. E. Lawler¹, C. Sneden², J. J. Cowan³, J.-F. Wyart⁴, I. I. Ivans⁵, J. S. Sobeck², M. H. Stockett¹,
and E. A. Den Hartog¹

¹Department of Physics, University of Wisconsin, Madison, WI 53706; jelawler@wisc.edu,
stockett@wisc.edu, eadenhar@wisc.edu

²Department of Astronomy and McDonald Observatory, University of Texas, Austin, TX
78712; chris@verdi.as.utexas.edu, jsobeck@astro.as.utexas.edu

³Department of Physics and Astronomy, University of Oklahoma, Norman, OK 73019; cowan@nhn.ou.edu

⁴Laboratoire Aimé Cotton, Centre National de la Recherche Scientifique (UPR3321), 91405-
Orsay, France; Jean-Francois.Wyart@lac.u-psud.fr

⁵The Observatories of the Carnegie Institution of Washington, 813 Santa Barbara St., Pasadena,
CA 91101 & Princeton University Observatory, Peyton Hall, Princeton, NJ 08544; iii@ociw.edu

ABSTRACT

Recent radiative lifetime measurements accurate to $\pm 5\%$ (Stockett et al. 2007, J. Phys. B 40, 4529) using laser-induced fluorescence (LIF) on 8 even-parity and 62 odd-parity levels of Er II have been combined with new branching fractions measured using a Fourier transform spectrometer (FTS) to determine transition probabilities for 418 lines of Er II. This work moves Er II onto the growing list of rare earth spectra with extensive and accurate modern transition probability measurements using LIF plus FTS data. This improved laboratory data set has been used to determine a new solar photospheric Er abundance, $\log \varepsilon = 0.96 \pm 0.03$ ($\sigma = 0.06$ from 8 lines), a value in excellent agreement with the recommended meteoric abundance, $\log \varepsilon = 0.95 \pm 0.03$. Revised Er abundances have also been derived for the r -process-rich metal-poor giant stars CS 22892-052, BD+17°3248, HD 221170, HD 115444, and CS 31082-001. For these five stars the average Er/Eu abundance ratio, $\langle \log \varepsilon (\text{Er}/\text{Eu}) \rangle = 0.42$, is in very good agreement with the solar-system r -process ratio. This study has further strengthened the finding that r -process nucleosynthesis in the early Galaxy which enriched these metal-poor stars yielded a very similar pattern to the r -process which enriched later stars including the Sun.

Subject headings: atomic data — stars: abundances stars: Population II — Sun: abundances — Galaxy: evolution — nuclear reactions, nucleosynthesis, abundances — stars: individual (HD 115444, HD 221170, BD +17 3248, CS 22892-052, CS 31082-001, CS 29497-030)

1. INTRODUCTION

The study of elemental abundances in stellar photospheres continues to be a rich area of investigation. The availability of new large aperture telescopes has dramatically increased the number of target stars for which high spectral resolution data with a high signal-to-noise ratio can be obtained. One of the major successes in this area during recent years was the discovery and detailed study of a class of metal-poor Galactic halo stars with variable n (eutron)-capture elemental abundances (e.g. Sneden et al. 1995, Smith et al. 1995, Cowan et al. 1996, Sneden et al. 1996, Woolf et al. 1995, Sneden et al. 2000, Burris et al. 2000). Halo stars are among the oldest objects in the Galaxy, and provide a window on the earliest phases of Galactic evolution. The last decade has seen the first detection and abundance determination of numerous heavy elements in very metal-poor, n -capture rich halo stars, including the important chronometer uranium (Cayrel et al. 2001, Frebel et al. 2007).

Rare Earth (RE) elements are among the most spectroscopically accessible of the n -capture elements. The open f-shell of the RE neutral atoms and ions yields many strong lines in the visible and near-IR where spectral line blending is less of a problem than in the UV. Advantages from reduced blending in astrophysical data analysis are not matched by ease in calculating the basic atomic data needed for abundance determinations. These species with open f-shells have substantial relativistic effects causing a nearly complete breakdown of Russell-Saunders coupling¹. They also have many low-lying, overlapping configurations leading to extensive configuration interaction. In some cases there are hundreds to thousands of interacting levels that need to be included in accurate calculations on the strongest “resonance-like” transitions. Ab-initio quantum mechanical calculations on these spectra represent a formidable task even with the best currently available computers. The challenge of calculating spectroscopic data for RE neutral atoms and ions has attracted the attention of theorists (see Biémont & Quinet 2003 and references therein). In such complex spectra progress is being made through an interplay of theory and experiment. Often some experimental information is essential to “tune” theoretical methods.

The systematic determination of experimental transition probabilities by combining radiative lifetimes from time-resolved laser induced fluorescence (TR-LIF) with branching fractions from emission data recorded with a Fourier transform spectrometer (FTS) has played a central role in providing the basic atomic data needed for RE abundance determinations (e.g. Lawler 2006 and references therein). This method yields absolute transition probabilities which are accurate to $\pm 5\%$ (~ 0.02 dex) for strong lines. Improved laboratory data has reduced line-to-line and star-

¹ Russell-Saunders coupling applies for light atoms in which the Coulomb repulsion of electrons in the Hamiltonian overwhelms relativistic effects including spin-orbit, spin-other orbit, spin-spin, and orbit-orbit interactions. In most levels of light atoms the total electronic angular momentum operator \mathbf{L}^2 and total electronic spin \mathbf{S}^2 are diagonal, or yield very good quantum numbers. In RE atoms relativistic effects are typically comparable to, or larger than, Coulomb repulsion terms in the Hamiltonian. The only generally good quantum numbers for levels of light atoms and RE atoms are eigenvalues of the total electronic angular momentum $\mathbf{J}^2 = (\mathbf{L} + \mathbf{S})^2$ and parity operators.

to-star scatter in abundance values for many RE elements. The emergence of a tightly defined r -process only abundance pattern in many very metal-poor Galactic halo stars, at least for the RE elements, has been an exciting development (e.g. Sneden et al. 2003, Ivans et al. 2006, Lawler et al. 2006, Den Hartog et al. 2006). As this abundance pattern becomes even more tightly defined, it will: i) provide a powerful constraint on future modeling of the r -process nucleosynthesis; ii) help determine a definitive r -process site; and iii) unlock other details of the r -process and of the Galactic chemical evolution.

Erbium is one of the RE elements in need of additional work. There have been some LIF lifetime measurements (e.g. Bentzen et al. 1982, Xu et al. 2003, Xu et al. 2004), but a large set of experimental transition probabilities based on the best modern methods was not available before this work. Recent and extensive TR-LIF lifetime measurements by Stockett et al. (2007) provide a foundation for determining a large set of atomic transition probabilities from FTS data. We report the measurement of branching fractions for 418 lines of Er II and the determination of absolute transition probabilities for these lines by combining our branching fractions with radiative lifetime data from Stockett et al. (2007). These laboratory data are applied to re-determine the Solar abundance of Er and to refine the Er abundance in five r -process rich, metal poor Galactic halo stars.

2. ER II BRANCHING FRACTIONS AND ATOMIC TRANSITION PROBABILITIES

The availability of large and accurate set of radiative lifetimes from Stockett et al. (2007) provides a foundation for this study of branching fractions and the transition probabilities of Er II. A very powerful spectrometer is essential for branching fraction measurements on rich RE spectra. As in earlier work on RE spectra, we used the 1.0 meter FTS at the National Solar Observatory (NSO) for branching fraction measurements in this project. This instrument has the large etendue of all interferometric spectrometers, a limit of resolution as small as 0.01 cm^{-1} , wavenumber accuracy to 1 part in 10^8 , broad spectral coverage from the UV to IR, and the capability of recording a million point spectrum in 10 minutes (Brault 1976). An FTS is insensitive to any small drift in source intensity since an interferogram is a simultaneous measurement of all spectral lines.

2.1 Energy Levels of Er II

One of the challenges in this undertaking is the lack of configuration and term assignments for most observed levels of Er II. Figure 1 shows a partial Grotrian diagram constructed from the compilation of Martin et al. (1978) for this ion. A total of 117 even-parity and 243 odd-parity levels are included in the compilation. The substantial overlap of low configurations leads to extensive configuration interaction and makes definitive assignments quite difficult for many levels. The lack of level assignments causes only minor difficulties in experimental work on branching fractions and transition probabilities since one cannot guess the strongest branches from an upper level. However, the lack of level assignments makes ab-initio theoretical determination of transition probability data very difficult.

Configuration and term assignments are firm for the lowest 26 levels of the 117 known even-parity levels including: 12 levels of the $4f^{12}(^3H)6s_{1/2}$ and $4f^{12}(^3F)6s_{1/2}$ sub-configurations, 10 levels of the $4f^{12}(^3H_6)5d_{3/2}$ and $4f^{12}(^3H_6)5d_{5/2}$ sub-configurations, and 4 levels $4f^{12}(^3F_4)5d_{3/2}$ sub-configurations. Fortunately this list of low even-parity levels with firm assignments is nearly complete below $\sim 20,000 \text{ cm}^{-1}$. Although there is a missing $4f^{12}(^1G)6s_{1/2}^2$ G term in the 15,000 to 20,000 cm^{-1} range, the nearly complete list of even-parity levels $< 20,000 \text{ cm}^{-1}$ reduces concerns of possible strong branches to unobserved low even-parity levels affecting the accuracy of our branching fraction measurements from upper odd-parity levels. Above 20,000 cm^{-1} there are numerous unobserved even-parity levels. Between 25,000 cm^{-1} and 31,000 cm^{-1} there are only 9 levels assigned to the $4f^{12}(^3H)5d$ sub-configuration and these lack term assignments. Except for the 9 levels of the $4f^{11}(^3H_{15/2})6s6p(^3P)$ sub-configuration between 32,000 cm^{-1} and 38,000 cm^{-1} the remaining even-parity levels are either tentatively assigned to the $4f^{11}(^4I)5d6p$ sub-configuration or in most cases unassigned. A new analysis of Er II is underway (Wyart et al. 2008 to be submitted).

The fraction of observed levels with assignments is somewhat lower for the 243 known odd-parity levels. Only the lowest odd-parity level at 6825 cm^{-1} and two higher levels have firm term assignments. These three levels are part of the low 4I term of $4f^{11}6s^2$ configuration. Another 28 levels starting from 10,667 cm^{-1} have firm assignments to the $4f^{11}(^4I)5d6s$ sub-configuration and seven have tentative assignments to this sub-configuration. These 38 levels are the lower levels of strong branches from the upper even-parity levels included in our branching fraction study. There are 10 additional levels ranging from 25,000 cm^{-1} to 34,000 cm^{-1} with tentative term and configuration assignments to the $4f^{12}6p$ configuration. All other odd-parity levels lack both term and configuration assignments. The ongoing reanalysis of Er II indicates the lowest unobserved odd-parity level is just under 20,000 cm^{-1} (Wyart et al. 2008 to be submitted). There are quite a number of unobserved odd-parity levels in the 20,000 cm^{-1} to 30,000 cm^{-1} range. These levels, like many of the upper odd-parity levels included in our branching fraction study, are mixtures of states from $4f^{12}6p$, $4f^{11}6s^2$, $4f^{11}5d6s$, and $4f^{11}5d^2$ configurations.

The crucial issue in this review of assignments for low Er II levels is whether or not there are significant branches from upper levels in this study to unobserved lower levels. Although many previously unobserved levels have been located in the ongoing reanalysis of Er II (Wyart et al. 2008 to be submitted), these levels are very weakly connected to upper levels of this study with one exception. We will return to the issue of unobserved levels after discussing our branching fraction measurements.

2.2 Er II Branching Fraction Analysis and Relative Radiometric Calibration

As in earlier studies our experimental branching fractions are based on a large set of FTS data including: spectra of lamps at high currents to reveal very weak branches to known levels, good IR spectra to reveal any significant IR branches to known levels, and low current spectra in which dominant branches are optically thin covering the UV to near-IR. Table 1 is a list of the 15 FTS spectra used in our branching fraction study. All were recorded using the National Solar

Observatory 1.0 meter FTS on Kitt Peak. Some of these spectra (#1-6, 12-15) were recorded by other guest observers in the 1980's, and others (#7-11) were recorded during our February 2000 and February 2002 observing runs. All 15 raw spectra are available from the electronic archives of the National Solar Observatory².

The establishment of an accurate relative radiometric calibration or efficiency is critical to a branching fraction experiment. As indicated in Table 1, we made use of both standard lamp calibrations and Ar I and Ar II line calibrations in this Er II study. Tungsten (W) filament standard lamps are particularly useful near the Si detector cutoff in the 10,000 to 9,000 cm^{-1} range where the FTS sensitivity is changing rapidly as a function of wave number, and near the dip in sensitivity at 12,500 cm^{-1} from the aluminum coated optics. Tungsten lamps are not bright enough to be useful for FTS calibrations in the UV region, and UV branches typically dominate the decay of levels studied using our lifetime experiment. In general one must be careful when using continuum lamps to calibrate the FTS over wide spectral ranges, because the “ghost” of a continuum is a continuum. The Ar I and Ar II line technique, which is internal to the Hollow Cathode Discharge (HCD) Er/Ar lamp spectra, is still our preferred calibration technique. It captures the wavelength-dependent response of detectors, spectrometer optics, lamp windows, and any other components in the light path or any reflections which contribute to the detected signal (such as due to light reflecting off the back of the hollow cathode). This calibration technique is based on a comparison of well-known branching ratios for sets of Ar I and Ar II lines widely separated in wavelength, to the intensities measured for the same lines. Sets of Ar I and Ar II lines have been established for this purpose in the range of 4300 to 35000 cm^{-1} by Adams & Whaling (1981), Danzmann & Kock (1982), Hashiguchi & Hasikuni (1985), and Whaling et al. (1993). One of our best Er/Ar HCD spectra from 2002, and the Er/Ar HCD spectra from 1987 and 1988, were calibrated with both W standard lamp spectra recorded shortly before, or after, the HCD lamp spectra and using the Ar I and Ar II line technique. The Er/Ne spectra from the 1987 and 1988 could only be calibrated using W standard lamp. The older W lamp is a strip lamp calibrated as a spectral radiance ($\text{W}/(\text{m}^2 \text{ sr nm})$) standard, and the newer is a tungsten-quartz-halogen lamp calibrated as a spectral irradiance ($\text{W}/(\text{m}^2 \text{ nm})$ at a specified distance) standard. Neither of these W filament lamps is hot or bright enough to yield a reliable UV calibration, but they are useful in the visible and near IR for interpolation and as a redundant calibration.

All possible transition wave numbers between known energy levels of Er II satisfying both the parity change and $\Delta J = -1, 0, \text{ or } 1$ selection rules were computed and used during analysis of FTS data. Energy levels from Martin et al. (1978) were used to determine possible transition wave numbers. Levels from Martin et al. (1978) are available in electronic form from Martin et al. (2000)³. Systematic errors from missing branches to known lower levels are negligible in our work, because we were able to make at least rough measurements on ultraviolet through IR lines

²Available at <http://nsokp.nso.edu/>

³Available at <http://physics.nist.gov/PhysRefData/ASD/index.html>

with branching fractions of 0.001 or smaller. This is illustrated in Table 2 which lists our branching fractions for the odd-parity upper level at $28361.386 \text{ cm}^{-1}$. For this level we were able to measure and report a very weak, 0.00040, branching fraction. Figures 2 and 3 show some Er II line profiles from this upper level. Figure 2 is the shortest wavelength, second strongest transition at 3524.905 \AA (branching fraction 0.389). Figure 3 is the second longest wavelength transition at 15458.105 \AA (branching fraction 0.00122). Given the large wavelength separation of these two lines, it should not be surprising that the data in Figures 2 and 3 are from different spectra. Isotopic structure is clearly visible in the IR line of Figure 3. The triplet pattern is due to the even (nuclear spin $I = 0$) isotopes ^{166}Er (abundance 33.61%), ^{168}Er (abundance 26.78%), and ^{170}Er (abundance 14.93%) (Rossman & Taylor 1997). Hyperfine structure “smears out” the transition of the other abundant Er isotope which is the odd ($I = 7/2$) isotope ^{167}Er (abundance 22.93%) and individual hyperfine components from this odd isotope are difficult to detect in our spectra. The two lightest isotopes, ^{164}Er (abundance 1.61%) and ^{162}Er (abundance 0.14%), have such low abundances that they are not detectable in our spectra. Isotopic splittings are somewhat larger in the IR than in the UV for lines studied, but one should keep in mind that the FTS data of Figure 3 has higher spectral resolution than that of Figure 2. The IR lines with relatively large isotope shifts are very weak and have such large excitation potentials that we see no hope of detecting the lines in astrophysical spectra for the foreseeable future.

Branching fraction measurements were attempted on lines from all 80 levels of the lifetime experiment by Stockett et al. (2007), and were completed for lines from 7 even-parity and 63 odd-parity upper levels. The levels for which branching fractions could not be completed had a strong branch beyond the UV limit of our spectra, or had a strong branch which was severely blended. Typically an odd-parity upper level, depending on its J value, has about 20 possible transitions to known lower levels, and an even-parity upper level has about 60 possible transitions to known lower levels. More than 20,000 possible spectral line observations were studied during the analysis of 15 different Er/Ar and Er/Ne spectra. We set integration limits and occasionally nonzero baselines “interactively” during analysis of the FTS spectra. An occasional nonzero baseline is needed when a weak line is located on a line wing of a much stronger line. The same numerical integration routine was used to determine the un-calibrated intensities of Er II lines and selected Ar I and Ar II lines used to establish a relative radiometric calibration of the spectra. A simple numerical integration technique was used in this and most of our other RE studies because of weakly resolved or unresolved hyperfine and isotopic structure. More sophisticated profile fitting is used only when the line sub-component structure is either fully resolved in the FTS data or known from independent measurements.

2.3 Branching Fraction Uncertainties

The procedure for determining branching fraction uncertainties was described in detail by Wickliffe et al. (2000). Branching fractions from a given upper level are defined to sum to unity, thus a dominant line from an upper level has small branching fraction uncertainty almost by definition. Branching fractions for weaker lines near the dominant line(s) tend to have uncertainties limited

by their S/N ratios. Systematic uncertainties in the radiometric calibration are typically the most serious source of uncertainty for widely separated lines from a common upper level. We used a formula for estimating this systematic uncertainty that was presented and tested extensively by Wickliffe et al. (2000). The spectra of the high current custom HCD lamps enabled us to connect the stronger visible and near IR branches to quite weak branches in the same spectral range. Uncertainties grew to some extent from piecing together branching ratios from so many spectra, but such effects have been included in the uncertainties on branching fractions of the weak visible and near IR lines. In the final analysis, the branching fraction uncertainties are primarily systematic. Redundant measurements with independent radiometric calibrations help in the assessment of systematic uncertainties. Redundant measurements from spectra with different discharge conditions also make it easier to spot blended lines and optically thick lines. Many of the strong lines in the UV and visible were optically thick in the spectra from the Custom HCD lamp operating at high current. These data were discarded during review of the branching ratio data before combining data from the various spectra to determine our final branching fractions.

As mentioned in §2.1, one of the more troubling systematic uncertainties is from possible branches to unobserved lower levels. We have checked for branches from upper levels in this study to previously unobserved lower levels using both an experimental search to tentatively identified lower levels, and using results from a parametric fit to the energy levels. With only one exception, the upper levels of this study are very weakly connected to the unobserved lower levels. Based on the reanalysis of Er II to date, only the highest upper level of this study, the even-parity level at 46757.780 cm^{-1} , is likely to have significant branches to unobserved odd-parity lower levels (Wyart et al. 2008 to be submitted). Transition probabilities from this upper level have been reduced by 7.7% (~ 0.03 dex) to correct for the branches to unobserved lower levels. This correction introduces some additional systematic uncertainty for the four lines from this upper level included in our study. The reanalysis indicates that the odd-parity upper level at 33307.365 cm^{-1} has $J = 3.5$ ($7/2$ in standard notation) instead of 4.5 ($9/2$) as given in the NIST tables (Martin et al. 1978)⁴. The Landé g-factor supports this change. Careful inspection of all spectra in this study revealed some weak lines from this upper level to $J = 2.5$ ($5/2$) lower level and not a hint of a transition to a lower level with $J = 5.5$ ($11/2$). We therefore use the modified $J = 3.5$ ($7/2$) for the level at 33307.365 cm^{-1} and note that this change does not affect our Einstein A-coefficients from this upper level, but does affect the $\log(gf)$ values from this upper level. The reanalysis also indicates that the $J = 4.5$ ($9/2$) odd-parity level at 33129.912 cm^{-1} is not real. Only a single emission line at 3570.75 \AA from this upper level was detected in our branching fraction study, and this level does not fit in the parametric study of Er II (Wyart et al. to be submitted). The lifetime of 4.7 ns reported by Stockett et al. (2007) is correct for laser excitation at 3570.75 \AA , but no transition probabilities can be reported until the J and actual energy of the upper level is established.

⁴ Redundant decimal notation and standard fractional notation for J values are included in the text, but our tables use only decimal notation required for the main machine readable table of transition probabilities.

2.4 Er II Atomic Transition Probabilities

Branching fractions from the FTS spectra were combined with the radiative lifetime measurements (Stockett et al. 2007) to determine absolute transition probabilities for 418 lines of Er II in Table 3. Air wavelengths in Table 3 were computed from energy levels (Martin et al. 1978) using the standard index of air (Edlén 1953). Parities are included in Table 3 using “ev” and “od” notation which is compatible with our main machine table of transition probabilities.

Transition probabilities for the very weakest lines (branching fractions ~ 0.001 or weaker) which were observed with poor S/N ratios and for a few blended lines are not included in Table 3, however these lines are included in the branching fraction normalization. The effect of the problem lines becomes apparent if one sums all transition probabilities in Table 3 from a chosen upper level, and compares the sum to the inverse of the upper level lifetime from Stockett et al. (2007). Typically the sum of the Table 3 transition probabilities is between 95% and 100 % of the inverse lifetime. Although there is significant fractional uncertainty in the branching fractions for these problem lines, this does not have much effect on the uncertainty of the stronger lines that were kept in Table 3. Branching fraction uncertainties are combined in quadrature with lifetime uncertainties to determine the transition probability uncertainties in Table 3.

There are only a few comparisons which can be made between our transition probability data and other similar data. The most interesting comparison is to the experimental work of Musiol and Labuz (1983) shown in Figure 4. The discordant points of Figure 4 may be, in some cases, due to incorrect line identifications from the lower resolving power achieved in the earlier grating spectrometer measurements by Musiol and Labuz. In complex rare earth spectra, the resolution and absolute wavenumber accuracy of a FTS is extremely important. Line broadening and blending could also have been a problem in the experiments by Musiol and Labuz because they used a high pressure (LTE) arc plasma. Lines from our low pressure HCD lamps are primarily Doppler broadened in most cases. Although the comparison to Musiol and Labuz is not as favorable as one might hope, it is better than the comparisons to theoretical results in Figures 5 and 6. Figures 5 and 6 are, respectively, comparisons of our results against relativistic Hartree Fock calculations (Xu et al. 2003) and semi-empirical results from Kurucz (2007). It is important to recall that the very comprehensive Kurucz database was originally intended for opacity calculations, and not for precise spectroscopic research. (It should also be noted that some of the Kurucz data is from Labuz and Musiol.) Calculations of transition probabilities in Er II are indeed a very difficult theoretical undertaking. We note that the reanalysis of Er II is yielding encouraging results. Theoretical branching fractions are in good agreement with experimental branching fractions for all of the even-parity upper levels in this study, and for about half of the odd-parity upper levels. In the next sections we apply our new laboratory results in Er abundance determinations.

3. SOLAR AND STELLAR ERBIUM ABUNDANCES

The new transition probabilities have been applied to Er II lines in the solar photosphere and

five very metal-poor ($[\text{Fe}/\text{H}] < -2$)⁵ stars that have large overabundances of the rare earth elements. Our abundance study followed the methods used for Hf II by Lawler et al. (2007) and previous papers in this series. Erbium has been less well studied in solar/stellar spectra than have many other rare earth ions, due to a lack of extensive previous lab investigations and to a paucity of transitions in spectral regions convenient for ground-based high resolution spectroscopy. Anecdotal evidence to support this suggestion comes from the classic Moore, Minnaert, & Houtgast (1966) solar line compendium. Those authors could identify only 2 Er II transitions (at 3896.2 Å and 3903.3 Å), in contrast with the large number they identified for many other rare-earth ions (e.g. 146 Sm II and 72 Gd II lines). Identification of a suitable set of Er II lines was therefore as important as the subsequent abundance analysis.

3.1 Line Selection

We have accurate transition probabilities for 418 Er II lines, but only a small minority of these can be employed to determine Er abundances in the Sun and our chosen metal-poor stars. This is because all strong Er II lines occur only in the near-UV spectral domain, $\lambda < 4000$ Å. As discussed by Lawler et al. (2007 and references therein), to first approximation the relative strengths of weak-to-moderate lines within one species depend directly on their transition probabilities modified by the Boltzmann excitation factors. For a line on the linear part of the curve-of-growth the relationship between equivalent width EW, reduced width RW, transition probability, excitation energy χ (measured in eV), and inverse temperature $\theta \equiv 5040/T$ is:

$$\log(\text{RW}) = \log(\text{EW}/\lambda) = \text{constant} + \log(gf) - \theta\chi/g$$

The relative strengths of lines of different species also depend on relative elemental abundances and Saha ionization equilibrium factors. However, the relatively low first ionization potential of Er (6.108 eV, Grigoriev & Melikhov 1997) ensures that it almost entirely exists as Er II in the photospheres of the Sun and stars considered here. Therefore Er II, like those of all rare-earth single ions, needs essentially no Saha corrections for the existence of other ionization states. Thus for all elements with similarly low ionization potentials their weak-ionized-line strength factors are

$$\text{STR} \equiv \log(\varepsilon gf) - \theta\chi,$$

where ε is the elemental abundance.

In Figure 7 we plot these relative strength factors as a function of wavelength for Gd II lines (Den Hartog et al. 2006) and Er II lines (this paper). To compute the strength factors we have adopted solar abundances of $\log \varepsilon(\text{Gd}) = +1.11$ (Den Hartog et al.) and $\log \varepsilon(\text{Er}) = +0.95$ (close to the recommended photospheric abundance of Grevesse & Sauval 2002 and Lodders 2003) which will be the new value derived in this paper. This plot is very similar to ones that we have shown in several of our previous papers. As in those studies we have used horizontal lines to indicate

⁵ We adopt standard stellar spectroscopic notations that for elements A and B, $[A/B] = \log_{10}(N_A/N_B)_{\text{star}} - \log_{10}(N_A/N_B)_{\text{sun}}$, for abundances relative to solar, and $\log \varepsilon(A) = \log_{10}(N_A/N_H) + 12.0$, for absolute abundances.

approximate strength factors for “strong” and “barely detectable” lines as follows.

The minimum detectable strength limit for Sm II lines was estimated by Lawler et al. (2006) by first searching the Delbouille et al. (1973) solar photospheric spectrum for the weakest lines that could be reliably employed in an abundance analysis. That exercise suggested an EW limit of about 1.5 mÅ near $\lambda \sim 4500 \text{ \AA}$, or $\log(\text{RW}) \approx -6.5$. Lines of Sm II near this limit had have $\text{STR} = \log(\varepsilon gf) - \theta_\chi \approx -0.6$. That EW and thus STR limit should apply also to Gd II and Er II lines, and so it has been indicated in both panels of Figure 7 with horizontal dotted lines.

Minimum strength factors for relatively strong lines were estimated by Lawler et al. (2006) by beginning with the detection-limit $\text{STR} = -0.6$ and increasing it by a factor of 20, or $\text{STR} = -0.6 + 1.3 = +0.7$. Ignoring curve-of-growth saturation effects would imply that $\log(\text{RW}) = -6.5 + 1.3 = -5.2$ (or $\text{EW} \approx 30 \text{ mÅ}$ near 4500 \AA). Such lines actually are slightly saturated, and tests with the solar spectrum suggested $\log(\text{RW}) \approx -5.35$, or $\text{EW} \approx 20 \text{ mÅ}$ at 4500 \AA for $\text{STR} = +0.7$. We have drawn dashed horizontal lines to indicate this “strong-line” limit in Figure 7.

This study has reported transition probabilities of Er II lines with wavelengths nearly as long as $20,000 \text{ \AA}$ (2μ), but Figure 7 displays only the regime $2900 \text{ \AA} \leq \lambda \leq 6000 \text{ \AA}$. This is because all of the Er II lines beyond 6000 \AA have $\text{STR} < -1.7$, more than 1 dex weaker than our estimated minimum detectability threshold of $\text{STR} = -0.6$. In fact, the right-hand panel of this figure shows that very few Er II lines should even be detectable in the solar spectrum longward of 4000 \AA . We have drawn vertical lines at 4000 \AA in the figure to bring attention to this difficulty. Nearly 75 Gd II lines longward of 4000 \AA have $\text{STR} \geq -0.6$, while just 6 Er II lines qualify. All strong Er II lines are located in the complex near-UV spectral domain, where line blending from other species might compromise even the most promising Er II transition.

As discussed in Lawler et al. (2007) and earlier papers, the strength factors of Figure 7 provided the first cut in paring the list of 418 Er II lines to a useful set for solar/stellar work. Some 115 lines survived the $\text{STR} \geq -0.6$ test. We then followed Lawler et al. to identify the final set of potentially useful Er II lines. Using the Delbouille et al. (1973) solar center-of-disk spectrum, the Moore et al. (1966) solar line identifications, the comprehensive Kurucz (1998)⁶ atomic and molecular line lists, and the spectrum of the r -process-rich metal-poor giant star CS 22892-052 (Snedden et al. 2003), we eliminated all but 57 Er II lines; the rest proved to be too weak and/or too blended (see Lawler et al. 2006 for specific examples of the process). The CS 22892-052 spectrum was especially helpful in this exercise, as the combined effects of its very low metallicity ($[\text{Fe}/\text{H}] \approx -3.1$) and large neutron-capture r -process excess (e.g., $[\text{Eu}/\text{Fe}] \approx +1.6$) creates very favorable conditions for Er II line detection. If a candidate line is unusable in the CS 22892-052 spectrum, it almost certainly will not be available for a solar analysis.

We then computed preliminary synthetic spectra for the surviving Er II lines. As in Lawler et al. (2006), we assembled atomic and molecular line lists in small (4-6 Å) wavelength regions, beginning

⁶Available at <http://kurucz.harvard.edu/>

with Kurucz’s (1998) line database and Moore et al.’s (1966) solar identifications. For many neutron-capture ionized species we used gf -values from recently published studies: Y, Hannaford et al. (1982); Zr, Malcheva et al. (2006); La, Lawler et al. (2001a); Ce, Palmeri et al. (2000); Nd, Den Hartog et al. (2003); Sm, Lawler et al. (2006); Eu, Lawler et al. (2001b); Gd, Den Hartog et al. (2006); Tb, Lawler et al. (2001c); Dy, Wickliffe et al. (2000); Ho, Lawler et al. (2004); Er, the present paper; and Hf, Lawler et al. (2007). We adopted the Holweger & Müller (1974) solar empirical model photosphere, and the CS 22892-052 model interpolated from the Kurucz grid by Sneden et al. (2003). For solar computations we used a standard solar abundance set (e.g. Grevesse & Sauval 1998, 2002; Lodders 2003), modified to include recent updates for the neutron-capture elements, and for CS 22892-052 we used abundances from Sneden et al. (2003), modified for neutron-capture elements by our previous papers in this series.

Line lists, model atmospheres, and abundance sets were input into the current version of the LTE line analysis code MOOG (Sneden 1973) to generate initial synthetic spectra. Empirical Gaussian broadening functions were applied to smooth the synthetic spectra to match the effects of solar/stellar macroturbulence and spectrograph instrumental profile. Visual inspection of the synthetic/observed spectrum matches were sufficient to reduce the 57 candidate lines to 23 that were suitable for abundance analysis in the Sun and/or CS 22892-052. These transitions were the ones examined in all program stars.

3.2 The Solar Photospheric Erbium Abundance

We computed multiple synthetic spectra for each Er line region in a more careful manner, trying to account for the details of the solar spectra. As discussed in §2, Er II lines in the red-IR have detectable hyperfine/isotopic substructure (Figure 3), but it is negligible for the near-UV lines (e.g., Figure 2) that we used for solar/stellar abundances. Therefore we treated these lines as single absorbers. The oscillator strengths for atomic lines other than the neutron-capture species referenced in §3.1 were adjusted to fit the solar spectrum. Abundances of elements C, N, and O were altered to match the strengths of observed CH, CN, NH, and OH lines. Of course many solar absorption features, especially in the near-UV spectral region of greatest interest in this study, remain unidentified. We arbitrarily declared these lines to be Fe I with excitation potentials $\chi = 3.5$ eV and gf -values adjusted to fit the solar spectrum. We compared these iterated synthetic spectra to the Delbouille et al. (1973) center-of-disk photospheric spectrum. In any case where line contamination of identified or unknown origin proved to be a significant part of the overall absorption at the Er II wavelength, the line was discarded for the solar analysis but kept for possible use with the metal-poor giants.

The final solar Er abundance is based on eight Er II lines, whose individual abundances are listed in Table 4, column 4. These lines include the 3896.2 Å feature identified by Moore et al. (1966), but their 3903.3 Å line was not part of our laboratory investigation. In the top panel of Figure 8 we display the solar Er line abundances; no obvious trends with wavelength are apparent. A straight mean abundance is $\log \varepsilon(\text{Er}) = 0.96 \pm 0.02$ ($\sigma = 0.06$).

Abundance uncertainties have been described in earlier papers of this series. Here, we estimate line profile fitting uncertainties to be ± 0.02 dex, and uncertainties due to contamination by other species lines are ± 0.04 dex. The mean error in $\log(gf)$ for the eight lines used in the solar analysis (see Table 3) is ± 0.02 . Adding these uncertainties in quadrature yields an estimated total internal uncertainty per transition of ± 0.05 dex, which is close to the observed $\sigma = 0.06$.

Overall scale errors can be due to atomic data uncertainties beyond gf errors, and model atmosphere choices. Recalling that Saha-fraction corrections are negligible for Er II, the main atomic uncertainties would be Boltzmann factors, which vary with the partition functions. Irwin (1981) computed polynomial fits to partition functions that were generated with the atomic energy level data available at that time, and his formulae have been widely used in stellar line analysis programs. We re-calculated Er I and Er II partition functions with the most recent experimental energy level data (Martin et al. 1978, 2000), and found that the new values of $\log(U)$ are up to ~ 0.2 dex larger in the temperature domain of interest for this study. We have used the new partition functions from experimental energy levels for all of our abundances. A reanalysis of Er II, which is currently underway (Wyart et al. 2008 to be submitted), indicates that the remaining unobserved low-lying levels of each parity could further increase the partition function by 0.016 dex at 6000 K, but much less at lower temperature. This final theoretical correction to the Er II partition function is not included here because nearly all of the rare earth partition functions need similar adjustments due to unobserved levels.

As in Lawler et al. (2007), we repeated some of the abundance computations using the Kurucz (1998) and Grevesse & Sauval (1999) models, finding on average abundance shifts of -0.02 dex compared to those done with the Holweger & Müller (1974) model. Combining line-to-line scatter uncertainties (± 0.02 from the standard deviation of the mean, Table 4) with scale uncertainties, we recommend $\log \varepsilon(\text{Er})_{Sun} = +0.96 \pm 0.03$.

Biémont & Youssef (1984) provided the previous major solar Er investigation. From an equivalent width analysis of seven lines, they derived $\log \varepsilon(\text{Er})_{Sun} = +0.93 \pm 0.06$, in good agreement with our new value (only the 3781.0 Å and 3896.2 Å lines are in common between the two studies). Lodders (2003) adopts this abundance in her solar abundance review, and recommends a meteoritic value in even closer agreement with our value: $\log \varepsilon(\text{Er}) = +0.95 \pm 0.03$. This point will be considered again in §3.4.

In Figure 9 we compare solar-system meteoritic abundances with photospheric

abundances for the nine rare-earth elements studied in this series of papers. The meteoritic values are adopted from Lodders' (2003) compilation. References to the photospheric values are given in the figure caption. It is clear that the two data sets agree well: a simple mean offset is $+0.01 \pm 0.02$ ($\sigma = 0.05$). These numbers are consistent with error estimates on individual meteoritic and photospheric abundances.

3.3 Erbium Abundances in Five r -Process-Rich Low Metallicity Stars

We also derived Er abundances in five very metal-poor, r -process-rich giant stars: CS 22892-052 ($[\text{Fe}/\text{H}] = -3.1$, $[\text{Eu}/\text{Fe}] = +1.5$, Sneden et al. 2003); BD+17°3248 ($[\text{Fe}/\text{H}] = -2.1$, $[\text{Eu}/\text{Fe}] = +0.9$, Cowan et al. 2002); HD 221170 ($[\text{Fe}/\text{H}] = -2.2$, $[\text{Eu}/\text{Fe}] = +0.8$, Ivans et al. 2006); and HD 115444 ($[\text{Fe}/\text{H}] = -2.9$, $[\text{Eu}/\text{Fe}] = +0.8$, Westin et al. 2000); CS 31082-001 ($[\text{Fe}/\text{H}] = -2.9$, $[\text{Eu}/\text{Fe}] = +1.7$, Hill et al. 2002). Many Er II lines that are too blended and/or weak in the solar spectrum could be employed here, and we ended up with 14-21 lines contributing to the mean abundances. We derived Er abundances for the stars in the same manner as was described for the Sun in §3.2. The abundances from individual lines are listed in Table 4 and displayed in Figure 8. The mean abundances, standard deviations, and number of lines are given at the bottom of Table 4 and Figure 8. The line-to-line scatters are all small, $\sigma = 0.04 - 0.08$. The derived Er abundances show no noticeable dependence on wavelength, $\log(gf)$, or excitation potential.

4. DISCUSSION

The Er results are similar to those found for other RE studies, where the new experimental atomic data has dramatically reduced the scatter in star-to-star elemental abundance comparisons. We show this agreement and these comparisons in Figure 10. In the top panel of the figure we show the differential elemental abundance values for the four stars CS 22892-052, BD+17 3248, HD 221170 and HD 115444. In all cases the stars' elemental abundances have been scaled relative to Eu and the differences are with respect to the predicted solar system r -process only value. For these cases we have employed the r -process predictions from Simmerer et al. (2004) (see also Sneden, Cowan, & Gallino 2008). (A perfect agreement with the r -process only would fall on the dotted horizontal line in Figure 10.) Previous studies of the RE elements, including that of Nd (Den Hartog et al. 2003), Ho (Lawler et al. 2004), Sm (Lawler et al. 2006), and Gd (Den Hartog et al. 2006) and of the inter-peak element Hf (Lawler et al. 2007), have improved the precision of the stellar elemental abundances, as is apparent by the close agreement in the figure. The Er abundances for these four studied stars now are tightly clustered with relatively small error bars indicated in the bottom of the figure (as means of the sigmas for each element in the four stars) and are consistent with the solar system r -process only value.

Table 4 includes analyses for two additional stars. While not included in Figure 10 we have also analyzed the Er abundances in CS 31082-001. Previously we had determined the Hf abundance in this star (see Lawler et al. 2007). From 19 Er II lines we derive $\log \varepsilon(\text{Er}) = -0.30 \pm 0.01$ ($\sigma = 0.04$). With our own analysis of Eu II lines (Lawler et al. 2007) we find $\log \varepsilon(\text{Eu}) = -0.72$, and $\log \varepsilon(\text{Eu}/\text{Er}) = -0.42$. This value is essentially identical to the Eu/Er ratios found for the four other r -process rich stars. A more complete analysis is underway (Ivans et al. to be submitted). In contrast to these r -process rich stars we have also measured nine Er II lines in the star CS 29497-030, a star rich in both r - and s - process material (Ivans et al. 2005). We find $\log \varepsilon(\text{Er}) = +0.57 \pm 0.02$ ($\sigma = 0.07$), or $\log \varepsilon(\text{Eu}/\text{Er}) = -0.64$. The 0.2 dex difference in the ratio between this star and the other five stars results from the effects of changing from a pure r abundance to a mix of $r + s$.

Interestingly, it appears that the average Er abundance for the four r -process rich stars illustrated in Figure 10 lies just slightly above the scaled solar value. This might suggest that Er may be similar to the cases of Gd (Den Hartog et al. 2006) and Hf (Lawler et al. 2007), where the stellar data argue for a somewhat larger r -process fraction for the total solar system abundances (see also Sneden et al. 2008). Some of the remaining small systematic uncertainties, e.g. the correction of partition functions for unobserved levels, will further enhance the r -process abundances.

A few RE elements remain to be improved including Ce (Lawler et al., in preparation), but most of these elements have now been well studied. The Er results presented here, along with the other RE studies, have all led to much more precise stellar elemental abundances. These abundances in the metal-poor (r -process rich) halo stars are all consistent with a solar system r -process only origin. This study has further strengthened the finding that r -process nucleosynthesis in the early Galaxy which enriched these metal-poor stars yielded a very similar pattern to the r -process which enriched later stars including the Sun. This in turn provides important constraints on the timescales for such synthesis - that is it suggests rapidly evolving astronomical sites, forming the elements, ejecting them and mixing them into the interstellar medium, all prior to the formation of the halo stars - and points to the (possibly massive) nature of the first stars.

ACKNOWLEDGEMENTS

This work has been supported by the National Science Foundations through grants AST-0506324 to JEL & EDH, AST- 0607708 to CS, and AST-0707447 to JJC.

REFERENCES

- Adams, D. L., & Whaling, W. 1981, *J. Opt. Soc. Am.*, 71, 1036
- Bentzen, S. M., Nielsen, U., & Poulsen, O. 1982, *J. Opt. Soc. Am.*, 72, 1210
- Biémont, E. & Youssef, N. Y. 1984, *A&A*, 140, 177
- Biémont, E. & Quinet P. 2003, *Physica Scripta*, T105, 38
- Brault, J. W. 1976, *J. Opt. Soc. Am.*, 66, 1081
- Burris D. L., Pilachowski C.A., Armandroff T. E., Sneden C., Cowan J. J., & Roe H. 2000, *ApJ*, 544, 302
- Cayrel R., Hill V., Beers T. C., Barbuy B., Spite M., Spite F., Plez B., Andersen J., Bonifacio P., Francois P., Molaro P., Nordstrom B., & Primas F. 2001, *Nature* 409, 691
- Cowan J. J., Sneden C., Truran J. W., & Burris D. L. 1996, *ApJ*, 460, L115
- Cowan, J. J., Sneden, C., Burles, S., Ivans, I. I., Beers, T. C., Truran, J. W., Lawler, J. E., Primas, F., Fuller, G. M., Pfeiffer, B., & Kratz, K.-L. 2002, *ApJ*, 572, 861
- Danzmann K., & Kock M. 1982, *J. Opt. Soc. Am.*, 72, 1556
- Delbouille, L, Roland, G., & Neven, L. 1973, *Photometric Atlas of the Solar Spectrum from lambda 3000 to lambda 10000*, (Liège, Inst. d'Ap., Univ. de Liège)
- Den Hartog, E. A., Lawler, J. E., Sneden, C., & Cowan, J. J. 2003, *ApJS*, 148, 543
- Den Hartog E. A., Lawler J. E., Sneden C., & Cowan J. J. 2006, *ApJS*, 167, 292
- Edlén, B. 1953, *J. Opt. Soc. Am.*, 43, 339
- Frebel A., Christlieb N., Norris J. E., Thom C., Beers T. C., & Rhee J. 2007, *ApJ*, 660, L117
- Grevesse, N., & Sauval, A. J. 1998, *Space Sci. Rev.*, 85, 161
- Grevesse, N., & Sauval, A. J. 1999, *A&A*, 347, 348
- Grevesse, N., & Sauval, A. J. 2002, *Adv. Space. Res.*, 30, 3
- Grevesse, N., Asplund, M., & Sauval, A. J. 2007, *Space Sci. Rev.*, 130, 105
- Grigoriev, I. S., & Melikhov, E. Z. 1997, *Handbook of Physical Quantities*, (Boca Raton, CRC Press) p. 516
- Hannaford, P., Lowe, R. M., Grevesse, N., Biémont, E., & Whaling, W. 1982, *ApJ*, 261, 736
- Hashiguchi, S., & Hasikuni, M. 1985, *J. Phys. Soc. Japan* 54, 1290
- Hill, V., et al. 2002, *A&A*, 387, 560

- Holweger, H., & Müller, E. A. 1974, *Sol. Phys.*, 39, 19
- Irwin, A. W. 1981, *ApJS*, 45, 621
- Ivans, I. I., Simmerer, J., Sneden, C., Lawler, J. E., Cowan, J. J., Gallino, R., & Bisterzo, S. 2006, *ApJ*, 645, 613
- Ivans, I. I., Sneden, C., Gallino, R., Cowan, J. J., & Preston, G. W. 2005, *ApJ*, 627, L145
- Kurucz, R. L. 1998, in *Fundamental Stellar Properties: The Interaction between Observation and Theory*, IAU Symp. 189, ed T. R. Bedding, A. J. Booth and J. Davis (Dordrecht: Kluwer), p. 217
- Kurucz R. L. 2007, 7. Linelists (<http://kurucz.harvard.edu/>)
- Lawler, J. E., Bonvallet, G., & Sneden, C. 2001a, *ApJ*, 556, 452
- Lawler, J. E., Wickliffe, M. E., Den Hartog, E. A., & Sneden, C. 2001b, *ApJ*, 563, 1075
- Lawler, J. E., Wickliffe, M. E., Cowley, C. R., & Sneden, C. 2001c, *ApJS*, 137, 341
- Lawler, J. E., Sneden, C., & Cowan, J. J. 2004, *ApJ*, 604, 850
- Lawler J. E., Den Hartog E. A., Sneden C., & Cowan J. J. 2006, *ApJS*, 162, 227
- Lawler J. E., Den Hartog E. A., Labby Z. E., Sneden C., Cowan J. J., & Ivans I. I. 2007, *ApJS*, 169, 120
- Lodders, K. 2003, *ApJ*, 591, 1220
- Malcheva, G., Blagoev, K., Mayo, R., Ortiz, M., Xu, H. L., Svanberg, S., Quinet, P., & Biémont, E. 2006, *MNRAS*, 367, 754
- Martin, W.C., Zalubas, R., & Hagan, L. 1978, *Atomic Energy Levels The Rare Earth Elements*, NSRDS NBS 60 (Washington: U. S. G. P. O.) p. 174
- Martin, W. C., Sugar, J., & Musgrove, A. 2000, *NIST Atomic Spectra Database*, (<http://physics.nist.gov/PhysRefData/ASD/index.html>)
- Moore, C. E., Minnaert, M. G. J., & Houtgast, J. 1966, *The Solar Spectrum 2934 Å to 8770 Å*, NBS Monograph 61 (Washington: U.S. G. P. O.)
- Musiol K., & Labuz S. 1983, *Physica Scripta* 27, 422
- Palmeri, P., Quinet, P., Wyart, J.-F., & Biémont, E. 2000, *Physica Scripta*, 61, 323
- Rosman, K. J. R., & Taylor, P. D. P. 1998, *Pure Appl. Chem.*, 70, 217
- Smith V. V., Cunha K., & Lambert D. L. 1995, *AJ*, 110, 2827
- Sneden, C. 1973, *ApJ*, 184, 839

Sneden C., Basri G., Boesgard A. M., Brown J. A., Carney B. W., Kraft R. P., Smith V., & Suntzeff N. B. 1995, *Publ. of the Astron. Soc. of the Pacific* 107, 997

Sneden C., McWilliam A., Preston G. W., Cowan J. J., Burris D. L., & Armosky B. J. 1996, *ApJ*, 467, 819

Sneden C., Cowan J. J., Ivans I. I., Fuller G., S. Burles, T. C. Beers, and J. E. Lawler 2000, *ApJ*, 533, L139

Sneden C., Cowan J. J., & Lawler J. E. 2003, *Nuclear Phys.* A718, 29c

Sneden, C., Cowan, J. J., & Gallino, R. 2008, *ARAA*, in press

Stockett M. H., Den Hartog E. A., and Lawler J. E., 2007, *J. Phys. B: Atomic, Mol., & Opt. Phys.* 40, 4529

Xu H., Jiang Z., Zhang Z., Dai A., Svanberg S., Quinet P., & Biémont E. 2003, *J. Phys. B: Atomic, Mol., & Opt. Phys.* 36, 1771

Xu, H. L., Jiang, H. M., Liu, Q., Jiang Z. K., & Svanberg, S. 2004, *Chin. Phys. Lett.*, 21, 1720

Westin, J., Sneden, C., Gustafsson, B., & Cowan, J.J. 2000, *ApJ*, 530, 783

Whaling W., Carle M. T., & Pitt M. L. 1993, *J. Quant. Spectrosc. Radiat. Transfer* 50, 7

Wickliffe, M. E., Lawler, J. E., & Nave, G. 2000, *J. Quant. Spectrosc. Radiat. Transfer*, 66, 363

Woolf V. M., Tomkin J., & Lambert D. L. 1995, *ApJ*, 453, 660

FIGURE CAPTIONS

Figure 1: Partial Grotrian diagram for Er II. Upper and lower levels of both parities included in this study are shown.

Figure 2: FTS data from spectra #7 of Table 1. The Er II line near the center of the plot is from the odd-parity upper level at $28361.386 \text{ cm}^{-1}$ to the even-parity ground level at 0.000 cm^{-1} . This UV line at 3524.913 \AA is the second strongest branch from the upper level with a branching fraction of 0.389. There are Er I lines visible at a somewhat lower wavenumber and at a higher wavenumber near the left edge of the plot. Ringing from the apodization of the interferogram is visible as well as some weak isotopic structure near the base of the line.

Figure 3: FTS data from spectra #6 of Table 1. The Er II line near the center of the plot is from the odd-parity upper level at $28361.386 \text{ cm}^{-1}$ to the even-parity lower level at $21894.055 \text{ cm}^{-1}$. This IR line at 15458.105 \AA is the second weakest branch reported from the upper level with a branching fraction of 0.00122. The triplet structure is from the dominant even (nuclear spin $I = 0$) isotopes.

Figure 4: Comparison of experimental transition probabilities from Musiol and Labuz (1983) to our transition probabilities as function of our transition probability or $\log(gf)$, wavelength, and upper level energy.

Figure 5: Comparison of theoretical transition probabilities from Xu et al. (2003) to our transition probabilities as function of our transition probability or $\log(gf)$, wavelength, and upper level energy.

Figure 6: Comparison of theoretical transition probabilities from Kurucz (2007) to our transition probabilities as function of our transition probability or $\log(gf)$, wavelength, and upper level energy.

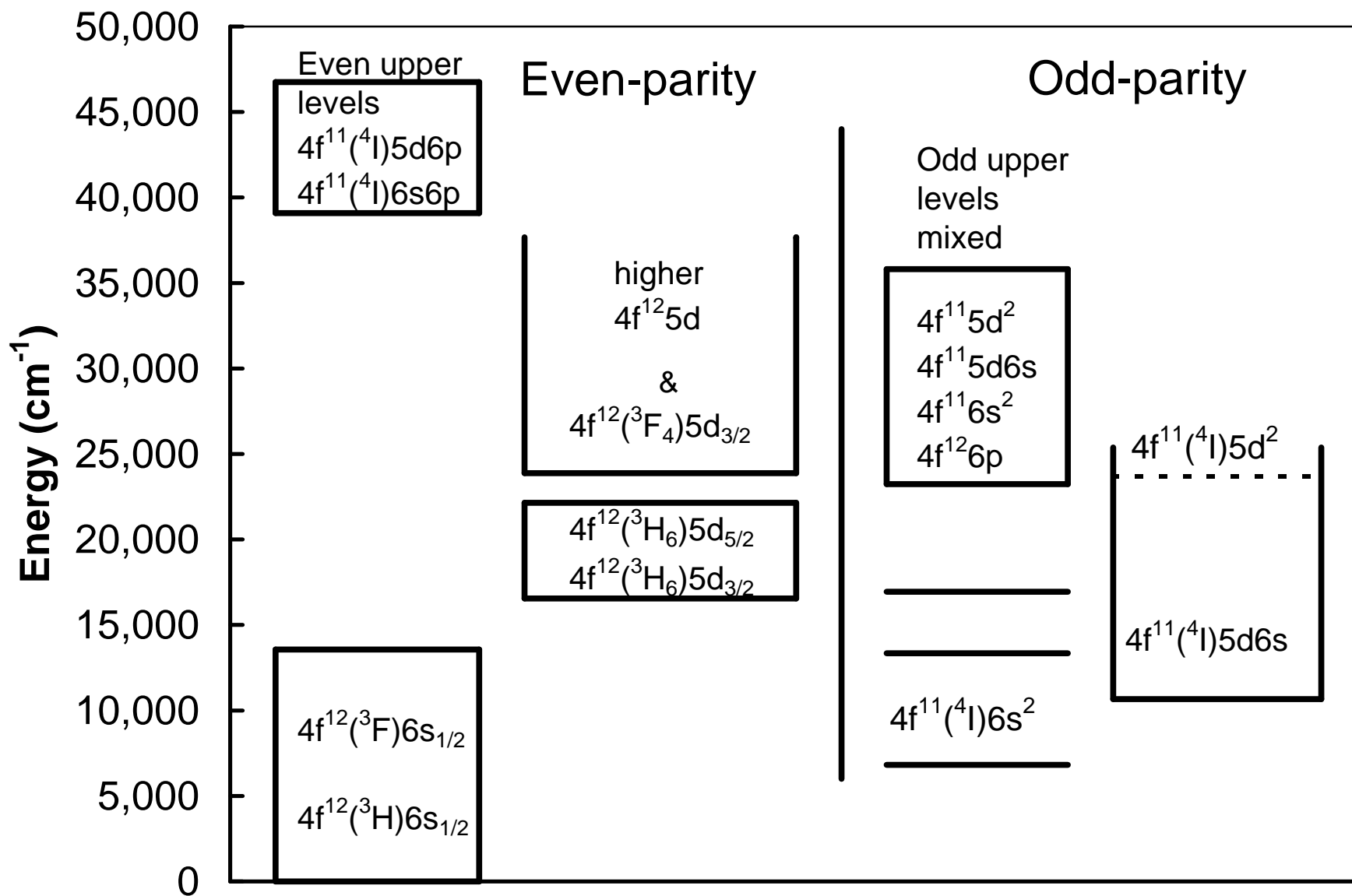
Figure 7: Relative transition strength factors, $\text{STR} \equiv \log(\varepsilon gf) - \theta\chi$, for lines of Gd II (Den Hartog et al. 2006) and Er II (this study). For display purposes the long-wavelength limit has been set to 6000 \AA , which cuts out only some extremely weak lines of Gd II and Er II that can be detected neither in the Sun nor nearly all other stars. The short-wavelength limit of 2900 \AA covers all lines at that end of the spectrum in these two studies. Definitions of “detection limit” and “strong lines” of these species are given in the text.

Figure 8: Line-by-line Er abundances for the Sun and the r -process-rich metal-poor giant stars CS 22892-052, BD+17°3248, HD 221170, HD 115444, and CS 31082-001, plotted as a function of wavelength. For each star, a dotted line is drawn at the mean abundance. As indicated in the figure legend, the three numbers in parentheses beside each star name are the mean abundance, the sample standard deviation σ , and the number of lines used in the analysis. The small scatter with an increased number of lines in comparison to earlier work (see text) yields improved accuracy and precision of abundance values.

Figure 9: Correlation of solar-system meteoritic and photospheric abundances for rare-earth elements studied in this series. The meteoritic abundances and their error estimates are those recommended by Lodders (2003). The sources of the photospheric abundances are: La, Lawler et al. (2001a); Nd, Den Hartog et al. (2003); Sm, Lawler et al. (2006); Eu, Lawler et al. (2001b); Gd, Den Hartog et al. (2006); Tb, Lawler et al. (2001c);

Ho, Lawler et al. (2004); Er, this study; and Hf, Lawler et al. (2007). Error bars adopted for the photospheric abundances are the sample standard deviations reported in those papers, which should be consulted for more detailed assessments. The dotted line indicates equality of the meteoritic and photospheric values. Note that a recently proposed renormalization by Grevesse, Asplund, & Sauval (2007) would decrease the meteoritic abundances uniformly by 0.03 dex.

Figure 10: Comparison of rare-earth abundances in four r -process-rich stars to the solar-system r -process-only abundances. The solar-system values are taken from Simmerer et al. (2004). The stars, identified in the figure legend, are those that have been analyzed in this series of papers. For each star, the abundance differences have been normalized such that $\Delta(\log \varepsilon(\text{Eu})) = 0$. The dotted line indicates equality between the stellar and solar-system r -only abundances. The error bars are the means of the sigma values of individual stellar abundances. The abundances for the named elements are taken from the present and earlier papers of this series, and other abundances are taken from the original stellar analyses of the stars.



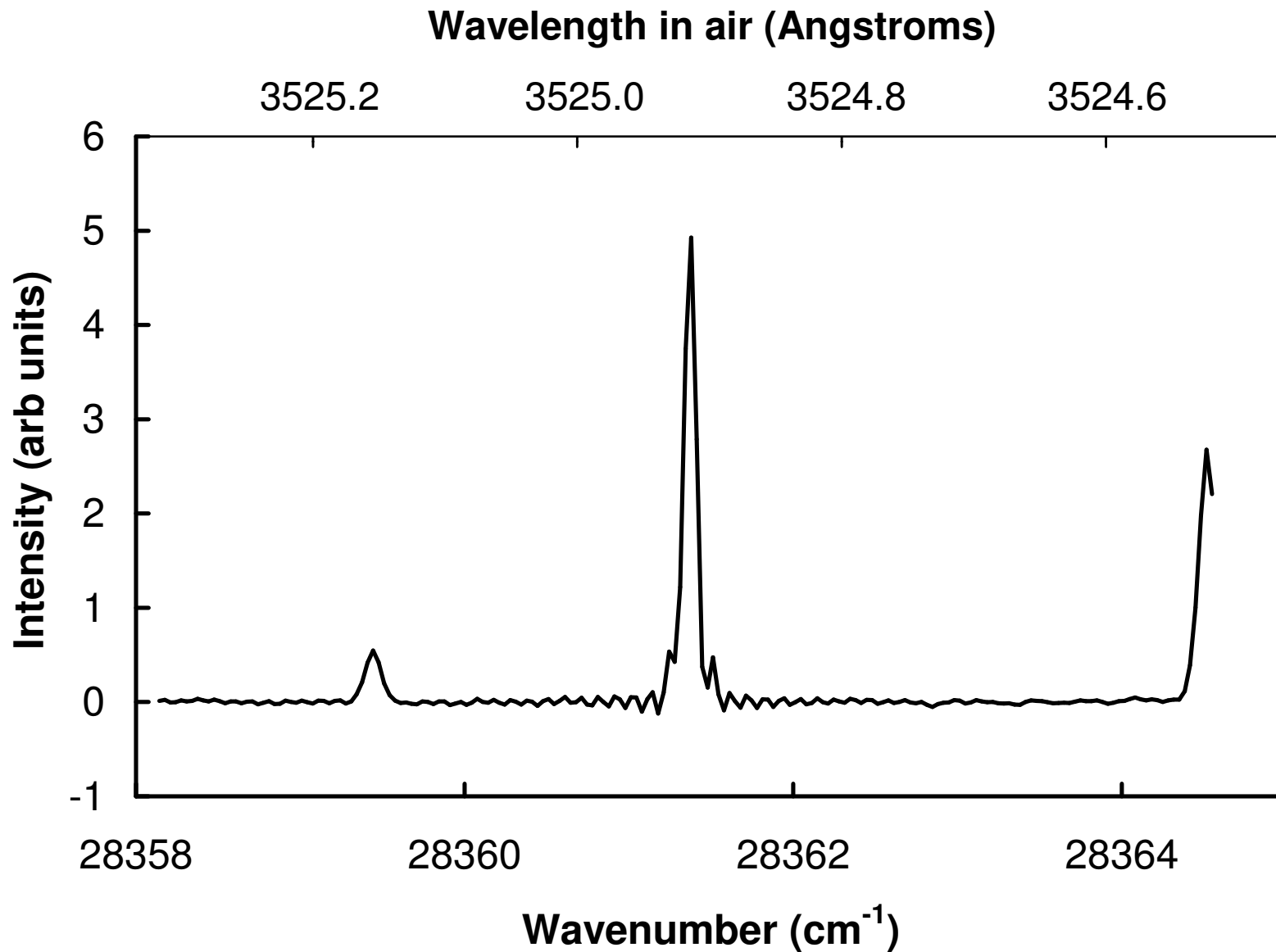


Table 2. Branching fractions for an odd-parity upper level of Er II organized by increasing wavelength in air, λ_{air} .

Wavenumber (cm^{-1})	λ_{air} (\AA)	E_{upper} (cm^{-1})	J_{upp}	E_{lower} (cm^{-1})	J_{low}	Branching Fraction
28361.39	3524.91	28361.39	5.5	0.00	6.5	0.389 ± 0.004
27920.95	3580.52	28361.39	5.5	440.43	5.5	0.569 ± 0.006
23228.78	4303.79	28361.39	5.5	5132.61	4.5	0.0100 ± 0.0009
21166.03	4723.23	28361.39	5.5	7195.35	4.5	0.0083 ± 0.0007
11808.51	8466.14	28361.39	5.5	16552.87	4.5	0.0098 ± 0.0018
9472.28	10554.22	28361.39	5.5	18889.10	5.5	0.0034 ± 0.0007
7633.34	13096.85	28361.39	5.5	20728.05	6.5	0.00040 ± 0.00010
6663.53	15002.95	28361.39	5.5	21697.85	5.5	0.0029 ± 0.0007
6467.33	15458.11	28361.39	5.5	21894.06	4.5	0.00122 ± 0.00029
6220.03	16072.70	28361.39	5.5	22141.35	6.5	0.0033 ± 0.0008

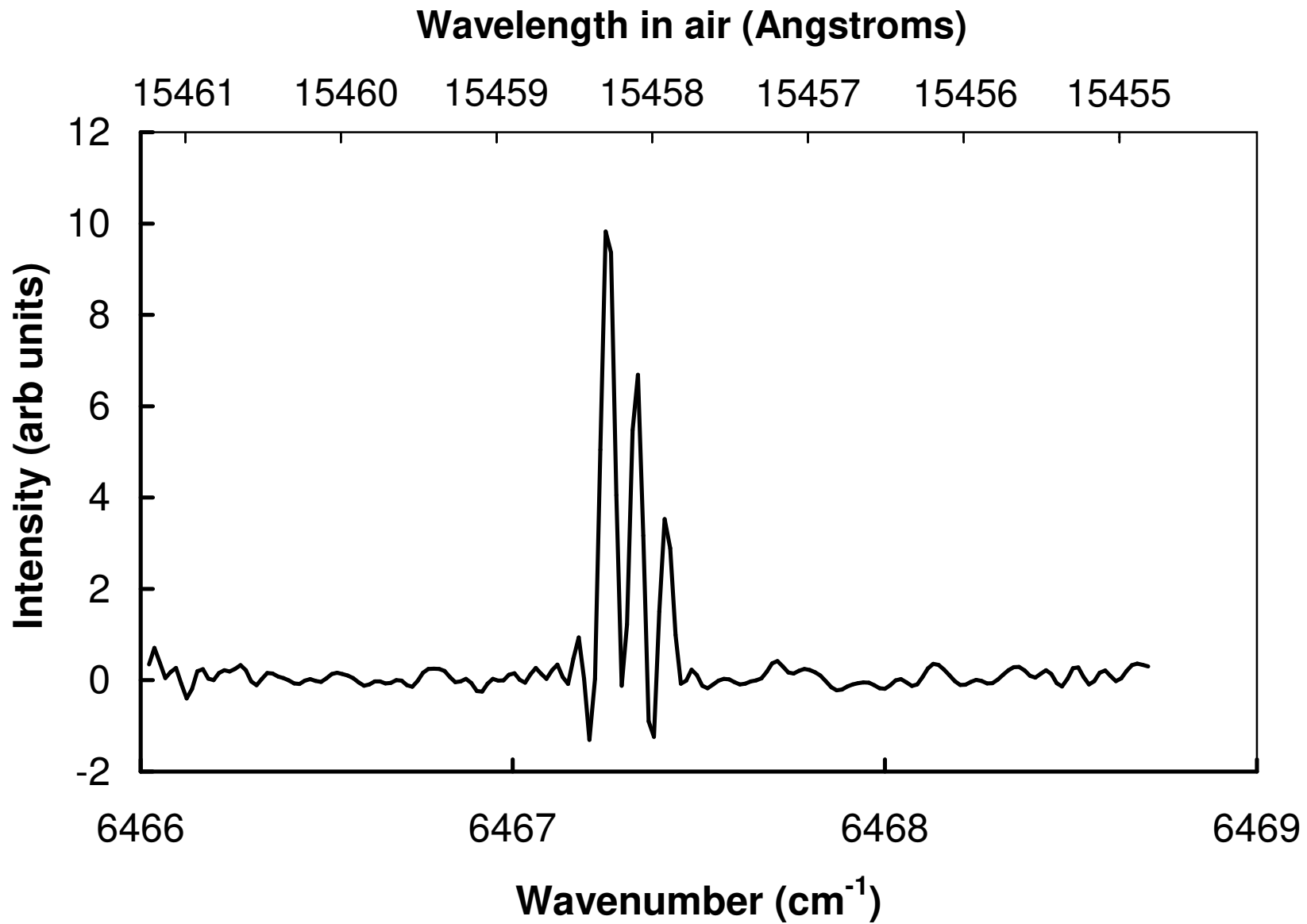


Table 3. Atomic transition probabilities for Er II organized by increasing wavelength in air, λ_{air} .

λ_{air} (Å)	E_{upper} (cm^{-1})	Parity	J_{upp}	E_{lower} (cm^{-1})	Parity	J_{low}	A-value (10^6 s^{-1})	$\log(gf)$
2892.398	34563.257	od	5.5	0.000	ev	6.5	0.26 ± 0.04	-2.41
2904.468	41244.400	ev	8.5	6824.774	od	7.5	93 ± 5	0.33
2910.362	41174.705	ev	7.5	6824.774	od	7.5	204 ± 11	0.62
2911.067	34341.611	od	5.5	0.000	ev	6.5	1.12 ± 0.18	-1.77
2920.240	34674.173	od	4.5	440.434	ev	5.5	1.56 ± 0.16	-1.70
2929.733	34563.257	od	5.5	440.434	ev	5.5	2.49 ± 0.28	-1.41
2941.329	33988.301	od	5.5	0.000	ev	6.5	0.58 ± 0.07	-2.05
2944.065	34397.143	od	4.5	440.434	ev	5.5	2.1 ± 0.3	-1.57
2945.280	46757.780	ev	9.5	12815.068	od	9.5	46.9 ± 2.9	0.09
2964.520	40547.199	ev	8.5	6824.774	od	7.5	159 ± 8	0.58
2968.761	33674.250	od	6.5	0.000	ev	6.5	9.5 ± 0.5	-0.75
2970.059	33659.536	od	5.5	0.000	ev	6.5	1.73 ± 0.23	-1.56
2972.275	34074.875	od	4.5	440.434	ev	5.5	3.36 ± 0.25	-1.35
2979.946	33988.301	od	5.5	440.434	ev	5.5	1.03 ± 0.13	-1.79
3002.406	40121.685	ev	6.5	6824.774	od	7.5	130 ± 7	0.39
3003.832	33721.545	od	5.5	440.434	ev	5.5	1.76 ± 0.12	-1.54
3008.107	33674.250	od	6.5	440.434	ev	5.5	0.322 ± 0.027	-2.21
3009.439	33659.536	od	5.5	440.434	ev	5.5	0.44 ± 0.05	-2.14
3012.472	46757.780	ev	9.5	13572.118	od	10.5	47 ± 3	0.11

3019.763	33105.534	od	5.5	0.000	ev	6.5	1.74 ± 0.17	-1.54
3025.919	46757.780	ev	9.5	13719.584	od	8.5	36.4 ± 2.1	0.00
3028.275	33012.493	od	6.5	0.000	ev	6.5	4.95 ± 0.25	-1.02
3031.309	39804.224	ev	7.5	6824.774	od	7.5	26.3 ± 2.3	-0.24
3046.871	32811.006	od	5.5	0.000	ev	6.5	0.27 ± 0.05	-2.34
3064.830	32618.753	od	5.5	0.000	ev	6.5	0.75 ± 0.08	-1.90
3066.221	37736.569	od	4.5	5132.608	ev	4.5	12.8 ± 1.2	-0.74
3069.224	33012.493	od	6.5	440.434	ev	5.5	2.09 ± 0.12	-1.38
3073.344	32528.401	od	6.5	0.000	ev	6.5	12.4 ± 0.6	-0.61
3080.206	32896.371	od	4.5	440.434	ev	5.5	0.52 ± 0.07	-2.13
3091.929	37736.569	od	4.5	5403.688	ev	3.5	2.62 ± 0.24	-1.43
3094.497	37438.656	od	4.5	5132.608	ev	4.5	0.59 ± 0.10	-2.07
3106.781	32618.753	od	5.5	440.434	ev	5.5	3.68 ± 0.27	-1.19
3113.537	46757.780	ev	9.5	14649.277	od	9.5	73 ± 4	0.33
3115.529	32528.401	od	6.5	440.434	ev	5.5	2.77 ± 0.18	-1.25
3116.948	32073.360	od	5.5	0.000	ev	6.5	3.48 ± 0.18	-1.22
3122.722	37146.674	od	5.5	5132.608	ev	4.5	3.60 ± 0.26	-1.20
3141.095	32267.246	od	4.5	440.434	ev	5.5	4.4 ± 0.3	-1.19
3143.634	31801.102	od	5.5	0.000	ev	6.5	1.84 ± 0.10	-1.49
3160.348	32073.360	od	5.5	440.434	ev	5.5	3.94 ± 0.21	-1.15
3160.786	36761.150	od	4.5	5132.608	ev	4.5	2.28 ± 0.19	-1.47
3181.920	31418.481	od	6.5	0.000	ev	6.5	17.5 ± 0.9	-0.43
3183.418	31844.124	od	4.5	440.434	ev	5.5	12.5 ± 0.8	-0.72

3185.247	31385.667	od	5.5	0.000	ev	6.5	5.8 ± 0.3	-0.98
3187.786	31801.102	od	5.5	440.434	ev	5.5	3.07 ± 0.16	-1.25
3188.112	36761.150	od	4.5	5403.688	ev	3.5	1.11 ± 0.09	-1.77
3227.161	31418.481	od	6.5	440.434	ev	5.5	3.04 ± 0.17	-1.18
3230.583	31385.667	od	5.5	440.434	ev	5.5	92 ± 5	0.24
3237.977	36007.182	od	4.5	5132.608	ev	4.5	19.1 ± 1.0	-0.52
3246.344	35927.604	od	3.5	5132.608	ev	4.5	0.45 ± 0.06	-2.25
3257.734	35819.939	od	3.5	5132.608	ev	4.5	3.01 ± 0.19	-1.42
3264.781	30621.102	od	6.5	0.000	ev	6.5	69 ± 3	0.19
3266.659	36007.182	od	4.5	5403.688	ev	3.5	6.1 ± 0.4	-1.01
3268.427	37736.569	od	4.5	7149.630	ev	5.5	3.9 ± 0.5	-1.21
3273.321	37736.569	od	4.5	7195.355	ev	4.5	9.2 ± 0.7	-0.83
3275.176	35927.604	od	3.5	5403.688	ev	3.5	1.06 ± 0.15	-1.87
3280.217	30917.436	od	4.5	440.434	ev	5.5	16.2 ± 0.8	-0.58
3286.769	35819.939	od	3.5	5403.688	ev	3.5	35.9 ± 1.8	-0.33
3300.575	37438.656	od	4.5	7149.630	ev	5.5	2.81 ± 0.25	-1.34
3305.566	37438.656	od	4.5	7195.355	ev	4.5	32.1 ± 1.7	-0.28
3312.426	30621.102	od	6.5	440.434	ev	5.5	40.9 ± 2.1	-0.03
3314.944	30157.742	od	5.5	0.000	ev	6.5	1.09 ± 0.06	-1.66
3318.774	30122.939	od	5.5	0.000	ev	6.5	1.80 ± 0.12	-1.45
3323.194	35215.487	od	5.5	5132.608	ev	4.5	34.3 ± 1.9	-0.17
3332.703	37146.674	od	5.5	7149.630	ev	5.5	59 ± 3	0.07
3337.791	37146.674	od	5.5	7195.355	ev	4.5	24.6 ± 1.3	-0.31

3339.586	41244.400	ev	8.5	11309.180	od	7.5	2.36 ± 0.26	-1.15
3340.026	35063.892	od	4.5	5132.608	ev	4.5	13.6 ± 0.7	-0.64
3346.034	30317.974	od	4.5	440.434	ev	5.5	25.6 ± 1.3	-0.37
3348.141	29858.739	od	5.5	0.000	ev	6.5	2.71 ± 0.14	-1.26
3358.153	34902.323	od	3.5	5132.608	ev	4.5	9.9 ± 0.5	-0.88
3364.076	30157.742	od	5.5	440.434	ev	5.5	18.5 ± 0.9	-0.42
3368.020	30122.939	od	5.5	440.434	ev	5.5	18.8 ± 0.9	-0.42
3370.553	35063.892	od	4.5	5403.688	ev	3.5	18.5 ± 0.9	-0.50
3372.752	29640.863	od	7.5	0.000	ev	6.5	145 ± 7	0.60
3374.170	29628.405	od	6.5	0.000	ev	6.5	15.2 ± 0.8	-0.44
3376.094	36761.150	od	4.5	7149.630	ev	5.5	9.5 ± 0.5	-0.79
3378.757	30028.618	od	4.5	440.434	ev	5.5	0.48 ± 0.04	-2.09
3381.316	36761.150	od	4.5	7195.355	ev	4.5	34.1 ± 1.8	-0.23
3384.089	34674.173	od	4.5	5132.608	ev	4.5	2.71 ± 0.17	-1.33
3389.014	34902.323	od	3.5	5403.688	ev	3.5	0.92 ± 0.08	-1.90
3389.739	29492.329	od	5.5	0.000	ev	6.5	6.1 ± 0.3	-0.90
3391.987	29472.789	od	7.5	0.000	ev	6.5	28.3 ± 1.4	-0.11
3394.093	40121.685	ev	6.5	10667.186	od	6.5	11.8 ± 1.0	-0.54
3396.843	34563.257	od	5.5	5132.608	ev	4.5	11.1 ± 0.6	-0.64
3398.269	29858.739	od	5.5	440.434	ev	5.5	2.07 ± 0.10	-1.37
3406.956	29783.733	od	4.5	440.434	ev	5.5	1.23 ± 0.09	-1.67
3416.126	34397.143	od	4.5	5132.608	ev	4.5	2.65 ± 0.21	-1.33
3422.620	34341.611	od	5.5	5132.608	ev	4.5	1.00 ± 0.12	-1.68

3425.087	29628.405	od	6.5	440.434	ev	5.5	3.11 ± 0.16	-1.12
3433.128	29119.606	od	6.5	0.000	ev	6.5	2.10 ± 0.11	-1.28
3439.723	34196.388	od	4.5	5132.608	ev	4.5	0.58 ± 0.05	-1.98
3441.130	29492.329	od	5.5	440.434	ev	5.5	12.5 ± 0.6	-0.58
3448.066	34397.143	od	4.5	5403.688	ev	3.5	7.9 ± 0.5	-0.85
3464.528	33988.301	od	5.5	5132.608	ev	4.5	8.2 ± 0.5	-0.75
3469.722	40121.685	ev	6.5	11309.180	od	7.5	32.5 ± 2.3	-0.09
3469.803	36007.182	od	4.5	7195.355	ev	4.5	1.89 ± 0.17	-1.47
3472.108	34196.388	od	4.5	5403.688	ev	3.5	0.143 ± 0.016	-2.59
3479.414	35927.604	od	3.5	7195.355	ev	4.5	39.4 ± 2.0	-0.24
3485.853	29119.606	od	6.5	440.434	ev	5.5	8.6 ± 0.4	-0.66
3486.824	34074.875	od	4.5	5403.688	ev	3.5	12.1 ± 0.7	-0.66
3492.501	35819.939	od	3.5	7195.355	ev	4.5	7.4 ± 0.4	-0.96
3496.856	33721.545	od	5.5	5132.608	ev	4.5	11.1 ± 0.6	-0.61
3499.103	29011.015	od	4.5	440.434	ev	5.5	105 ± 5	0.29
3504.457	33659.536	od	5.5	5132.608	ev	4.5	1.36 ± 0.11	-1.52
3508.379	39804.224	ev	7.5	11309.180	od	7.5	44.3 ± 2.4	0.12
3515.999	33565.895	od	4.5	5132.608	ev	4.5	2.62 ± 0.15	-1.31
3516.488	41244.400	ev	8.5	12815.068	od	9.5	4.2 ± 0.4	-0.86
3518.176	39082.884	ev	6.5	10667.186	od	6.5	28.5 ± 1.5	-0.13
3524.913	28361.386	od	5.5	0.000	ev	6.5	7.2 ± 0.4	-0.79
3543.017	41244.400	ev	8.5	13027.927	od	8.5	20.7 ± 1.7	-0.15
3548.263	33307.365	od	3.5	5132.608	ev	4.5	12.9 ± 0.7	-0.71

3549.844	33565.895	od	4.5	5403.688	ev	3.5	27.2 ± 1.4	-0.29
3551.790	41174.705	ev	7.5	13027.927	od	8.5	11.9 ± 1.1	-0.44
3553.203	33539.273	od	3.5	5403.688	ev	3.5	12.0 ± 0.6	-0.74
3559.894	28082.701	od	6.5	0.000	ev	6.5	7.6 ± 0.4	-0.69
3573.865	33105.534	od	5.5	5132.608	ev	4.5	2.78 ± 0.17	-1.19
3580.518	28361.386	od	5.5	440.434	ev	5.5	10.5 ± 0.5	-0.62
3581.376	35063.892	od	4.5	7149.630	ev	5.5	1.89 ± 0.17	-1.44
3583.748	33028.394	od	4.5	5132.608	ev	4.5	0.49 ± 0.03	-2.02
3587.252	35063.892	od	4.5	7195.355	ev	4.5	2.50 ± 0.23	-1.32
3599.501	39082.884	ev	6.5	11309.180	od	7.5	52.2 ± 2.7	0.15
3600.790	32896.371	od	4.5	5132.608	ev	4.5	2.09 ± 0.17	-1.39
3604.707	40121.685	ev	6.5	12388.090	od	5.5	19.9 ± 1.6	-0.27
3604.897	40547.199	ev	8.5	12815.068	od	9.5	42 ± 3	0.17
3608.171	34902.323	od	3.5	7195.355	ev	4.5	3.39 ± 0.22	-1.28
3611.896	32811.006	od	5.5	5132.608	ev	4.5	0.079 ± 0.015	-2.73
3616.566	27642.658	od	5.5	0.000	ev	6.5	21.0 ± 1.1	-0.31
3616.617	28082.701	od	6.5	440.434	ev	5.5	3.43 ± 0.17	-1.03
3618.916	33028.394	od	4.5	5403.688	ev	3.5	16.2 ± 0.8	-0.50
3632.050	41244.400	ev	8.5	13719.584	od	8.5	20.6 ± 2.0	-0.13
3632.086	34674.173	od	4.5	7149.630	ev	5.5	12.7 ± 0.7	-0.60
3632.781	40547.199	ev	8.5	13027.927	od	8.5	12.1 ± 1.3	-0.37
3633.536	27513.555	od	6.5	0.000	ev	6.5	10.6 ± 0.5	-0.53
3636.295	32896.371	od	4.5	5403.688	ev	3.5	1.29 ± 0.09	-1.59

3637.160	32618.753	od	5.5	5132.608	ev	4.5	5.4 ± 0.3	-0.89
3638.130	34674.173	od	4.5	7195.355	ev	4.5	0.61 ± 0.04	-1.92
3641.270	41174.705	ev	7.5	13719.584	od	8.5	28.1 ± 2.9	-0.05
3646.782	34563.257	od	5.5	7149.630	ev	5.5	2.18 ± 0.12	-1.28
3652.585	32502.680	od	4.5	5132.608	ev	4.5	7.6 ± 0.4	-0.82
3652.875	34563.257	od	5.5	7195.355	ev	4.5	12.6 ± 0.7	-0.52
3669.015	34397.143	od	4.5	7149.630	ev	5.5	15.5 ± 0.8	-0.50
3675.182	34397.143	od	4.5	7195.355	ev	4.5	2.14 ± 0.12	-1.36
3676.508	34341.611	od	5.5	7149.630	ev	5.5	5.07 ± 0.27	-0.91
3682.701	34341.611	od	5.5	7195.355	ev	4.5	17.3 ± 0.9	-0.38
3684.278	32267.246	od	4.5	5132.608	ev	4.5	11.7 ± 0.6	-0.62
3689.124	32502.680	od	4.5	5403.688	ev	3.5	2.92 ± 0.16	-1.22
3692.649	27513.555	od	6.5	440.434	ev	5.5	67 ± 3	0.28
3694.308	40121.685	ev	6.5	13060.715	od	6.5	7.6 ± 0.7	-0.66
3696.249	34196.388	od	4.5	7149.630	ev	5.5	15.9 ± 0.8	-0.49
3702.508	34196.388	od	4.5	7195.355	ev	4.5	1.61 ± 0.13	-1.48
3707.638	41244.400	ev	8.5	14280.723	od	7.5	46 ± 4	0.23
3710.793	32073.360	od	5.5	5132.608	ev	4.5	0.78 ± 0.06	-1.71
3717.247	41174.705	ev	7.5	14280.723	od	7.5	8.7 ± 1.0	-0.54
3719.247	34074.875	od	4.5	7195.355	ev	4.5	2.20 ± 0.19	-1.34
3721.457	32267.246	od	4.5	5403.688	ev	3.5	2.14 ± 0.12	-1.35
3724.358	37736.569	od	4.5	10893.936	ev	3.5	14.1 ± 0.9	-0.53
3724.907	33988.301	od	5.5	7149.630	ev	5.5	6.9 ± 0.4	-0.77

3729.524	26805.448	od	5.5	0.000	ev	6.5	10.4 ± 0.5	-0.59
3731.265	33988.301	od	5.5	7195.355	ev	4.5	19.5 ± 1.0	-0.31
3733.585	39804.224	ev	7.5	13027.927	od	8.5	2.72 ± 0.25	-1.04
3734.583	26769.141	od	6.5	0.000	ev	6.5	1.64 ± 0.08	-1.32
3738.162	39804.224	ev	7.5	13060.715	od	6.5	46.8 ± 2.5	0.20
3742.640	31844.124	od	4.5	5132.608	ev	4.5	20.6 ± 1.1	-0.36
3744.984	39082.884	ev	6.5	12388.090	od	5.5	18.6 ± 1.0	-0.26
3745.106	37736.569	od	4.5	11042.640	ev	4.5	15.2 ± 0.9	-0.50
3748.677	31801.102	od	5.5	5132.608	ev	4.5	0.61 ± 0.05	-1.81
3762.303	33721.545	od	5.5	7149.630	ev	5.5	0.87 ± 0.07	-1.65
3766.157	37438.656	od	4.5	10893.936	ev	3.5	20.8 ± 1.2	-0.35
3768.788	33721.545	od	5.5	7195.355	ev	4.5	2.43 ± 0.16	-1.21
3769.011	33674.250	od	6.5	7149.630	ev	5.5	0.42 ± 0.05	-1.90
3771.103	33659.536	od	5.5	7149.630	ev	5.5	7.0 ± 0.4	-0.75
3777.619	33659.536	od	5.5	7195.355	ev	4.5	5.01 ± 0.27	-0.89
3781.012	31844.124	od	4.5	5403.688	ev	3.5	10.3 ± 0.5	-0.66
3784.472	33565.895	od	4.5	7149.630	ev	5.5	0.148 ± 0.022	-2.50
3786.836	26399.775	od	5.5	0.000	ev	6.5	11.7 ± 0.6	-0.52
3787.375	37438.656	od	4.5	11042.640	ev	4.5	8.9 ± 0.6	-0.72
3791.034	33565.895	od	4.5	7195.355	ev	4.5	0.30 ± 0.04	-2.19
3791.828	26805.448	od	5.5	440.434	ev	5.5	4.63 ± 0.24	-0.92
3794.865	33539.273	od	3.5	7195.355	ev	4.5	0.21 ± 0.03	-2.44
3797.057	26769.141	od	6.5	440.434	ev	5.5	3.07 ± 0.15	-1.03

3806.054	40547.199	ev	8.5	14280.723	od	7.5	6.2 ± 0.7	-0.61
3807.999	31385.667	od	5.5	5132.608	ev	4.5	0.43 ± 0.05	-1.95
3828.569	33307.365	od	3.5	7195.355	ev	4.5	0.271 ± 0.029	-2.32
3830.482	26098.972	od	6.5	0.000	ev	6.5	19.4 ± 1.0	-0.22
3832.586	39804.224	ev	7.5	13719.584	od	8.5	5.3 ± 0.4	-0.73
3841.787	39082.884	ev	6.5	13060.715	od	6.5	4.9 ± 0.4	-0.82
3851.086	26399.775	od	5.5	440.434	ev	5.5	0.364 ± 0.019	-2.01
3851.596	33105.534	od	5.5	7149.630	ev	5.5	8.6 ± 0.4	-0.64
3858.393	33105.534	od	5.5	7195.355	ev	4.5	18.5 ± 0.9	-0.30
3863.077	33028.394	od	4.5	7149.630	ev	5.5	5.3 ± 0.3	-0.93
3864.802	36761.150	od	4.5	10893.936	ev	3.5	23.3 ± 1.4	-0.28
3865.452	33012.493	od	6.5	7149.630	ev	5.5	0.20 ± 0.04	-2.20
3880.611	30894.447	od	3.5	5132.608	ev	4.5	31.3 ± 1.6	-0.25
3882.886	32896.371	od	4.5	7149.630	ev	5.5	31.6 ± 1.6	-0.15
3887.149	36761.150	od	4.5	11042.640	ev	4.5	10.1 ± 0.7	-0.64
3889.795	32896.371	od	4.5	7195.355	ev	4.5	4.99 ± 0.25	-0.95
3895.803	32811.006	od	5.5	7149.630	ev	5.5	4.46 ± 0.23	-0.91
3896.234	26098.972	od	6.5	440.434	ev	5.5	23.9 ± 1.2	-0.12
3902.758	32811.006	od	5.5	7195.355	ev	4.5	8.8 ± 0.4	-0.62
3906.312	25592.343	od	5.5	0.000	ev	6.5	48.2 ± 2.4	0.12
3918.346	30917.436	od	4.5	5403.688	ev	3.5	2.77 ± 0.19	-1.20
3921.880	30894.447	od	3.5	5403.688	ev	3.5	6.0 ± 0.3	-0.95
3939.186	32528.401	od	6.5	7149.630	ev	5.5	0.31 ± 0.04	-1.99

3943.182	32502.680	od	4.5	7149.630	ev	5.5	3.38 ± 0.19	-1.10
3950.307	32502.680	od	4.5	7195.355	ev	4.5	0.170 ± 0.015	-2.40
3969.437	30317.974	od	4.5	5132.608	ev	4.5	2.96 ± 0.22	-1.16
3974.717	25592.343	od	5.5	440.434	ev	5.5	4.93 ± 0.25	-0.85
3980.144	32267.246	od	4.5	7149.630	ev	5.5	3.13 ± 0.18	-1.13
3994.853	30157.742	od	5.5	5132.608	ev	4.5	0.41 ± 0.03	-1.93
4000.417	30122.939	od	5.5	5132.608	ev	4.5	0.228 ± 0.018	-2.18
4011.107	32073.360	od	5.5	7149.630	ev	5.5	0.193 ± 0.020	-2.25
4012.627	30317.974	od	4.5	5403.688	ev	3.5	1.26 ± 0.10	-1.52
4015.573	30028.618	od	4.5	5132.608	ev	4.5	3.63 ± 0.18	-1.06
4017.355	35927.604	od	3.5	11042.640	ev	4.5	1.53 ± 0.12	-1.53
4018.479	32073.360	od	5.5	7195.355	ev	4.5	0.60 ± 0.05	-1.76
4043.162	29858.739	od	5.5	5132.608	ev	4.5	0.050 ± 0.005	-2.83
4048.342	31844.124	od	4.5	7149.630	ev	5.5	5.6 ± 0.3	-0.86
4055.407	31801.102	od	5.5	7149.630	ev	5.5	1.08 ± 0.09	-1.50
4055.464	29783.733	od	4.5	5132.608	ev	4.5	10.3 ± 0.5	-0.60
4055.852	31844.124	od	4.5	7195.355	ev	4.5	1.69 ± 0.11	-1.38
4059.779	30028.618	od	4.5	5403.688	ev	3.5	6.2 ± 0.3	-0.81
4062.944	31801.102	od	5.5	7195.355	ev	4.5	0.89 ± 0.08	-1.58
4100.558	29783.733	od	4.5	5403.688	ev	3.5	4.81 ± 0.24	-0.92
4103.979	29492.329	od	5.5	5132.608	ev	4.5	0.49 ± 0.03	-1.83
4112.615	41244.400	ev	8.5	16935.832	od	9.5	9.2 ± 1.1	-0.38
4132.721	31385.667	od	5.5	7195.355	ev	4.5	0.154 ± 0.020	-2.32

4135.654	36761.150	od	4.5	12587.998	ev	3.5	0.89 ± 0.11	-1.64
4135.707	35215.487	od	5.5	11042.640	ev	4.5	0.31 ± 0.04	-2.03
4142.914	29263.402	od	3.5	5132.608	ev	4.5	9.2 ± 0.5	-0.72
4186.704	29011.015	od	4.5	5132.608	ev	4.5	0.41 ± 0.03	-1.97
4189.984	29263.402	od	3.5	5403.688	ev	3.5	4.59 ± 0.23	-1.01
4201.241	41174.705	ev	7.5	17378.917	od	6.5	1.52 ± 0.27	-1.19
4206.187	30917.436	od	4.5	7149.630	ev	5.5	0.140 ± 0.016	-2.43
4214.295	30917.436	od	4.5	7195.355	ev	4.5	0.107 ± 0.012	-2.54
4234.056	40547.199	ev	8.5	16935.832	od	9.5	0.51 ± 0.07	-1.61
4234.781	29011.015	od	4.5	5403.688	ev	3.5	1.14 ± 0.08	-1.51
4253.541	34397.143	od	4.5	10893.936	ev	3.5	0.28 ± 0.03	-2.12
4280.625	34397.143	od	4.5	11042.640	ev	4.5	0.219 ± 0.024	-2.22
4285.578	35927.604	od	3.5	12600.093	ev	2.5	0.75 ± 0.08	-1.78
4290.187	34196.388	od	4.5	10893.936	ev	3.5	0.157 ± 0.027	-2.36
4301.596	23240.649	od	5.5	0.000	ev	6.5	0.85 ± 0.04	-1.55
4303.208	35819.939	od	3.5	12587.998	ev	3.5	0.37 ± 0.04	-2.08
4303.794	28361.386	od	5.5	5132.608	ev	4.5	0.185 ± 0.019	-2.21
4305.450	35819.939	od	3.5	12600.093	ev	2.5	0.46 ± 0.05	-1.99
4315.021	30317.974	od	4.5	7149.630	ev	5.5	0.123 ± 0.015	-2.46
4316.391	39804.224	ev	7.5	16643.237	od	6.5	1.23 ± 0.14	-1.26
4317.741	34196.388	od	4.5	11042.640	ev	4.5	0.071 ± 0.011	-2.70
4323.554	30317.974	od	4.5	7195.355	ev	4.5	0.027 ± 0.006	-3.12
4345.072	30157.742	od	5.5	7149.630	ev	5.5	0.150 ± 0.015	-2.29

4353.724	30157.742	od	5.5	7195.355	ev	4.5	0.015 ± 0.002	-3.29
4369.595	30028.618	od	4.5	7149.630	ev	5.5	0.463 ± 0.027	-1.88
4378.345	30028.618	od	4.5	7195.355	ev	4.5	0.58 ± 0.03	-1.78
4384.692	23240.649	od	5.5	440.434	ev	5.5	0.88 ± 0.04	-1.52
4388.380	41244.400	ev	8.5	18463.347	od	7.5	5.4 ± 0.8	-0.55
4401.847	41174.705	ev	7.5	18463.347	od	7.5	1.66 ± 0.25	-1.11
4402.283	29858.739	od	5.5	7149.630	ev	5.5	0.016 ± 0.003	-3.26
4403.173	40547.199	ev	8.5	17842.682	od	8.5	4.7 ± 0.6	-0.61
4414.680	33539.273	od	3.5	10893.936	ev	3.5	0.151 ± 0.018	-2.45
4416.871	29783.733	od	4.5	7149.630	ev	5.5	0.053 ± 0.007	-2.81
4420.232	33659.536	od	5.5	11042.640	ev	4.5	0.025 ± 0.004	-3.06
4425.813	29783.733	od	4.5	7195.355	ev	4.5	0.092 ± 0.008	-2.57
4432.663	39082.884	ev	6.5	16529.413	od	5.5	1.35 ± 0.15	-1.25
4438.609	33565.895	od	4.5	11042.640	ev	4.5	0.068 ± 0.011	-2.70
4441.213	27642.658	od	5.5	5132.608	ev	4.5	0.183 ± 0.017	-2.19
4457.997	39804.224	ev	7.5	17378.917	od	6.5	0.68 ± 0.07	-1.49
4460.359	33307.365	od	3.5	10893.936	ev	3.5	0.126 ± 0.013	-2.52
4474.479	29492.329	od	5.5	7149.630	ev	5.5	0.232 ± 0.023	-2.08
4480.169	34902.323	od	3.5	12587.998	ev	3.5	0.71 ± 0.07	-1.77
4482.599	34902.323	od	3.5	12600.093	ev	2.5	0.35 ± 0.04	-2.07
4483.655	29492.329	od	5.5	7195.355	ev	4.5	0.291 ± 0.027	-1.98
4490.150	33307.365	od	3.5	11042.640	ev	4.5	0.70 ± 0.07	-1.77
4526.926	40547.199	ev	8.5	18463.347	od	7.5	3.8 ± 0.5	-0.68

4540.229	39082.884	ev	6.5	17063.735	od	5.5	1.37 ± 0.16	-1.23
4550.391	29119.606	od	6.5	7149.630	ev	5.5	0.072 ± 0.007	-2.51
4552.138	39804.224	ev	7.5	17842.682	od	8.5	10.7 ± 0.8	-0.28
4572.994	29011.015	od	4.5	7149.630	ev	5.5	0.236 ± 0.023	-2.13
4574.596	32896.371	od	4.5	11042.640	ev	4.5	0.181 ± 0.027	-2.24
4583.948	34397.143	od	4.5	12587.998	ev	3.5	0.137 ± 0.016	-2.37
4615.866	40121.685	ev	6.5	18463.347	od	7.5	1.12 ± 0.16	-1.30
4700.768	26399.775	od	5.5	5132.608	ev	4.5	0.037 ± 0.004	-2.83
4723.230	28361.386	od	5.5	7195.355	ev	4.5	0.152 ± 0.016	-2.21
4774.104	40547.199	ev	8.5	19606.715	od	8.5	0.40 ± 0.11	-1.61
4815.967	31801.102	od	5.5	11042.640	ev	4.5	0.016 ± 0.003	-3.17
4839.625	41174.705	ev	7.5	20517.717	od	7.5	0.88 ± 0.17	-1.31
4848.415	39082.884	ev	6.5	18463.347	od	7.5	2.29 ± 0.27	-0.95
4886.284	25592.343	od	5.5	5132.608	ev	4.5	0.41 ± 0.04	-1.75
4889.255	27642.658	od	5.5	7195.355	ev	4.5	0.049 ± 0.006	-2.68
4909.274	27513.555	od	6.5	7149.630	ev	5.5	0.093 ± 0.013	-2.33
4922.703	32896.371	od	4.5	12587.998	ev	3.5	0.142 ± 0.016	-2.29
4949.724	39804.224	ev	7.5	19606.715	od	8.5	1.25 ± 0.17	-1.13
4956.316	41174.705	ev	7.5	21004.060	od	6.5	1.22 ± 0.22	-1.14
4966.623	40121.685	ev	6.5	19992.895	od	5.5	5.6 ± 0.8	-0.54
4992.739	30917.436	od	4.5	10893.936	ev	3.5	0.125 ± 0.018	-2.33
5097.994	26805.448	od	5.5	7195.355	ev	4.5	0.062 ± 0.010	-2.54
5099.587	40121.685	ev	6.5	20517.717	od	7.5	0.71 ± 0.12	-1.41

5183.528	39804.224	ev	7.5	20517.717	od	7.5	1.10 ± 0.12	-1.15
5193.320	26399.775	od	5.5	7149.630	ev	5.5	0.035 ± 0.004	-2.77
5224.658	30028.618	od	4.5	10893.936	ev	3.5	0.035 ± 0.010	-2.85
5292.391	29783.733	od	4.5	10893.936	ev	3.5	0.123 ± 0.014	-2.29
5317.623	39804.224	ev	7.5	21004.060	od	6.5	0.76 ± 0.10	-1.29
5414.189	40121.685	ev	6.5	21656.831	od	5.5	0.98 ± 0.18	-1.22
5434.162	25592.343	od	5.5	7195.355	ev	4.5	0.043 ± 0.008	-2.64
5462.434	40121.685	ev	6.5	21819.914	od	5.5	4.4 ± 0.8	-0.56
5518.121	29011.015	od	4.5	10893.936	ev	3.5	0.157 ± 0.029	-2.14
5529.797	39082.884	ev	6.5	21004.060	od	6.5	0.51 ± 0.08	-1.49
5710.870	41174.705	ev	7.5	23669.096	od	6.5	3.1 ± 0.6	-0.61
5788.607	41244.400	ev	8.5	23973.877	od	7.5	1.08 ± 0.21	-1.01
5791.140	39082.884	ev	6.5	21819.914	od	5.5	1.8 ± 0.3	-0.90
5812.062	41174.705	ev	7.5	23973.877	od	7.5	1.3 ± 0.3	-0.99
5844.055	33659.536	od	5.5	16552.871	ev	4.5	0.19 ± 0.04	-1.93
6045.633	41244.400	ev	8.5	24708.113	od	9.5	1.8 ± 0.4	-0.76
6061.249	40547.199	ev	8.5	24053.517	od	8.5	1.30 ± 0.27	-0.89
6267.934	32502.680	od	4.5	16552.871	ev	4.5	0.43 ± 0.06	-1.59
6311.750	40547.199	ev	8.5	24708.113	od	9.5	0.13 ± 0.03	-1.84
6347.166	39804.224	ev	7.5	24053.517	od	8.5	2.7 ± 0.4	-0.58
6509.833	26399.775	od	5.5	11042.640	ev	4.5	0.008 ± 0.001	-3.21
6556.327	31801.102	od	5.5	16552.871	ev	4.5	0.27 ± 0.06	-1.68
6616.741	39082.884	ev	6.5	23973.877	od	7.5	2.1 ± 0.4	-0.71

6740.117	33721.545	od	5.5	18889.101	ev	5.5	0.085 ± 0.020	-2.16
6761.677	33674.250	od	6.5	18889.101	ev	5.5	0.37 ± 0.07	-1.45
6768.413	33659.536	od	5.5	18889.101	ev	5.5	0.27 ± 0.04	-1.66
6944.942	33012.493	od	6.5	18617.495	ev	7.5	0.16 ± 0.03	-1.79
7329.735	32528.401	od	6.5	18889.101	ev	5.5	0.58 ± 0.11	-1.18
7348.284	30157.742	od	5.5	16552.871	ev	4.5	0.082 ± 0.015	-2.10
7367.130	30122.939	od	5.5	16552.871	ev	4.5	0.071 ± 0.013	-2.16
7513.412	29858.739	od	5.5	16552.871	ev	4.5	0.038 ± 0.008	-2.41
7556.006	29783.733	od	4.5	16552.871	ev	4.5	0.058 ± 0.010	-2.30
7694.178	32896.371	od	4.5	19903.107	ev	3.5	0.21 ± 0.03	-1.73
7726.173	29492.329	od	5.5	16552.871	ev	4.5	0.118 ± 0.021	-1.90
7742.602	31801.102	od	5.5	18889.101	ev	5.5	0.043 ± 0.011	-2.33
7934.594	32502.680	od	4.5	19903.107	ev	3.5	0.080 ± 0.015	-2.12
7999.998	31385.667	od	5.5	18889.101	ev	5.5	0.119 ± 0.025	-1.86
8085.683	32267.246	od	4.5	19903.107	ev	3.5	0.076 ± 0.014	-2.13
8328.540	30621.102	od	6.5	18617.495	ev	7.5	0.73 ± 0.16	-0.97
8466.139	28361.386	od	5.5	16552.871	ev	4.5	0.18 ± 0.03	-1.63
8521.354	30621.102	od	6.5	18889.101	ev	5.5	0.57 ± 0.12	-1.06
8708.910	33012.493	od	6.5	21533.153	ev	7.5	0.108 ± 0.025	-1.77
8871.749	30157.742	od	5.5	18889.101	ev	5.5	0.037 ± 0.008	-2.28
9014.831	27642.658	od	5.5	16552.871	ev	4.5	0.43 ± 0.08	-1.20
9069.148	29640.863	od	7.5	18617.495	ev	7.5	0.14 ± 0.03	-1.56
9072.496	34902.323	od	3.5	23883.022	ev	2.5	0.072 ± 0.018	-2.15

9076.591	30917.436	od	4.5	19903.107	ev	3.5	0.17 ± 0.04	-1.68
9092.342	32528.401	od	6.5	21533.153	ev	7.5	0.25 ± 0.06	-1.36
9176.314	29783.733	od	4.5	18889.101	ev	5.5	0.031 ± 0.006	-2.40
9196.145	33012.493	od	6.5	22141.355	ev	6.5	0.056 ± 0.014	-2.00
9209.568	29472.789	od	7.5	18617.495	ev	7.5	0.19 ± 0.04	-1.42
9309.036	29628.405	od	6.5	18889.101	ev	5.5	0.17 ± 0.03	-1.51
9380.387	31385.667	od	5.5	20728.050	ev	6.5	0.25 ± 0.05	-1.40
9428.504	29492.329	od	5.5	18889.101	ev	5.5	0.069 ± 0.015	-1.96
9519.284	29119.606	od	6.5	18617.495	ev	7.5	0.080 ± 0.016	-1.82
9530.677	37438.656	od	4.5	26949.099	ev	3.5	0.26 ± 0.06	-1.46
9599.026	30317.974	od	4.5	19903.107	ev	3.5	0.64 ± 0.15	-1.05
9670.370	29640.863	od	7.5	19302.832	ev	8.5	5.3 ± 1.1	0.08
9750.971	26805.448	od	5.5	16552.871	ev	4.5	0.58 ± 0.10	-1.00
9830.188	29472.789	od	7.5	19302.832	ev	8.5	0.66 ± 0.13	-0.82
9895.092	31801.102	od	5.5	21697.852	ev	5.5	0.037 ± 0.009	-2.18
10091.059	31801.102	od	5.5	21894.055	ev	4.5	0.021 ± 0.005	-2.41
10105.334	30621.102	od	6.5	20728.050	ev	6.5	0.062 ± 0.015	-1.87
10152.693	26399.775	od	5.5	16552.871	ev	4.5	0.17 ± 0.04	-1.50
10319.417	31385.667	od	5.5	21697.852	ev	5.5	0.92 ± 0.20	-0.75
10349.402	31801.102	od	5.5	22141.355	ev	6.5	0.050 ± 0.012	-2.01
10532.732	31385.667	od	5.5	21894.055	ev	4.5	0.42 ± 0.10	-1.07
10554.223	28361.386	od	5.5	18889.101	ev	5.5	0.062 ± 0.013	-1.91
10601.896	30157.742	od	5.5	20728.050	ev	6.5	0.043 ± 0.010	-2.06

10641.170	30122.939	od	5.5	20728.050	ev	6.5	0.14 ± 0.03	-1.54
10843.506	30917.436	od	4.5	21697.852	ev	5.5	0.077 ± 0.018	-1.87
10976.463	29011.015	od	4.5	19903.107	ev	3.5	0.84 ± 0.18	-0.82
11000.570	30621.102	od	6.5	21533.153	ev	7.5	0.96 ± 0.22	-0.61
11059.564	25592.343	od	5.5	16552.871	ev	4.5	1.05 ± 0.19	-0.64
11216.731	29640.863	od	7.5	20728.050	ev	6.5	0.14 ± 0.04	-1.37
11232.431	29628.405	od	6.5	20728.050	ev	6.5	0.045 ± 0.012	-1.92
11237.854	27513.555	od	6.5	18617.495	ev	7.5	1.48 ± 0.30	-0.41
11420.801	27642.658	od	5.5	18889.101	ev	5.5	0.14 ± 0.03	-1.49
11432.317	29472.789	od	7.5	20728.050	ev	6.5	0.056 ± 0.014	-1.76
11591.764	27513.555	od	6.5	18889.101	ev	5.5	0.034 ± 0.009	-2.01
11597.589	30317.974	od	4.5	21697.852	ev	5.5	0.108 ± 0.028	-1.66
11789.578	30621.102	od	6.5	22141.355	ev	6.5	0.52 ± 0.13	-0.82
11817.250	30157.742	od	5.5	21697.852	ev	5.5	0.13 ± 0.03	-1.48
11866.066	30122.939	od	5.5	21697.852	ev	5.5	0.106 ± 0.026	-1.57
11867.711	30317.974	od	4.5	21894.055	ev	4.5	0.27 ± 0.07	-1.25
12097.825	30157.742	od	5.5	21894.055	ev	4.5	0.082 ± 0.020	-1.67
12330.565	29640.863	od	7.5	21533.153	ev	7.5	0.72 ± 0.19	-0.58
12349.541	29628.405	od	6.5	21533.153	ev	7.5	0.13 ± 0.03	-1.39
12471.036	30157.742	od	5.5	22141.355	ev	6.5	0.057 ± 0.015	-1.79
12525.415	30122.939	od	5.5	22141.355	ev	6.5	0.053 ± 0.014	-1.82
12591.591	29472.789	od	7.5	21533.153	ev	7.5	0.086 ± 0.022	-1.48
12591.978	32502.680	od	4.5	24563.288	ev	4.5	0.071 ± 0.018	-1.77

12628.634	26805.448	od	5.5	18889.101	ev	5.5	0.134 ± 0.030	-1.41
12727.096	32896.371	od	4.5	25041.268	ev	3.5	0.18 ± 0.04	-1.37
12826.089	29492.329	od	5.5	21697.852	ev	5.5	0.071 ± 0.017	-1.68
12886.983	32502.680	od	4.5	24745.034	ev	5.5	0.086 ± 0.022	-1.67
12976.791	32267.246	od	4.5	24563.288	ev	4.5	0.065 ± 0.018	-1.79
13096.850	28361.386	od	5.5	20728.050	ev	6.5	0.007 ± 0.002	-2.65
13157.285	29492.329	od	5.5	21894.055	ev	4.5	0.039 ± 0.010	-1.91
13290.327	32267.246	od	4.5	24745.034	ev	5.5	0.073 ± 0.019	-1.72
13310.744	26399.775	od	5.5	18889.101	ev	5.5	0.055 ± 0.013	-1.75
13330.563	29640.863	od	7.5	22141.355	ev	6.5	0.064 ± 0.017	-1.56
13352.744	29628.405	od	6.5	22141.355	ev	6.5	0.050 ± 0.013	-1.73
13670.236	29011.015	od	4.5	21697.852	ev	5.5	0.20 ± 0.05	-1.25
14047.103	29011.015	od	4.5	21894.055	ev	4.5	0.30 ± 0.08	-1.05
14733.270	27513.555	od	6.5	20728.050	ev	6.5	0.16 ± 0.04	-1.15
15002.952	28361.386	od	5.5	21697.852	ev	5.5	0.054 ± 0.013	-1.66
15458.105	28361.386	od	5.5	21894.055	ev	4.5	0.023 ± 0.005	-2.01
16072.699	28361.386	od	5.5	22141.355	ev	6.5	0.060 ± 0.015	-1.55
16449.917	26805.448	od	5.5	20728.050	ev	6.5	0.043 ± 0.010	-1.68
16716.718	27513.555	od	6.5	21533.153	ev	7.5	0.014 ± 0.004	-2.08
17173.441	29783.733	od	4.5	23962.378	ev	3.5	0.019 ± 0.005	-2.08
17190.131	27513.555	od	6.5	21697.852	ev	5.5	0.035 ± 0.009	-1.67
17372.398	30317.974	od	4.5	24563.288	ev	4.5	0.012 ± 0.003	-2.28
17626.507	26399.775	od	5.5	20728.050	ev	6.5	0.012 ± 0.003	-2.18

17938.951	30317.974	od	4.5	24745.034	ev	5.5	0.019 ± 0.006	-2.05
18172.549	27642.658	od	5.5	22141.355	ev	6.5	0.013 ± 0.003	-2.10
18609.267	27513.555	od	6.5	22141.355	ev	6.5	0.047 ± 0.013	-1.47
18664.940	32896.371	od	4.5	27540.195	ev	5.5	0.076 ± 0.019	-1.40
18907.775	32896.371	od	4.5	27608.985	ev	4.5	0.054 ± 0.014	-1.54
19150.227	29783.733	od	4.5	24563.288	ev	4.5	0.044 ± 0.012	-1.62
19801.920	29011.015	od	4.5	23962.378	ev	3.5	0.034 ± 0.010	-1.70
19840.977	29783.733	od	4.5	24745.034	ev	5.5	0.064 ± 0.015	-1.42

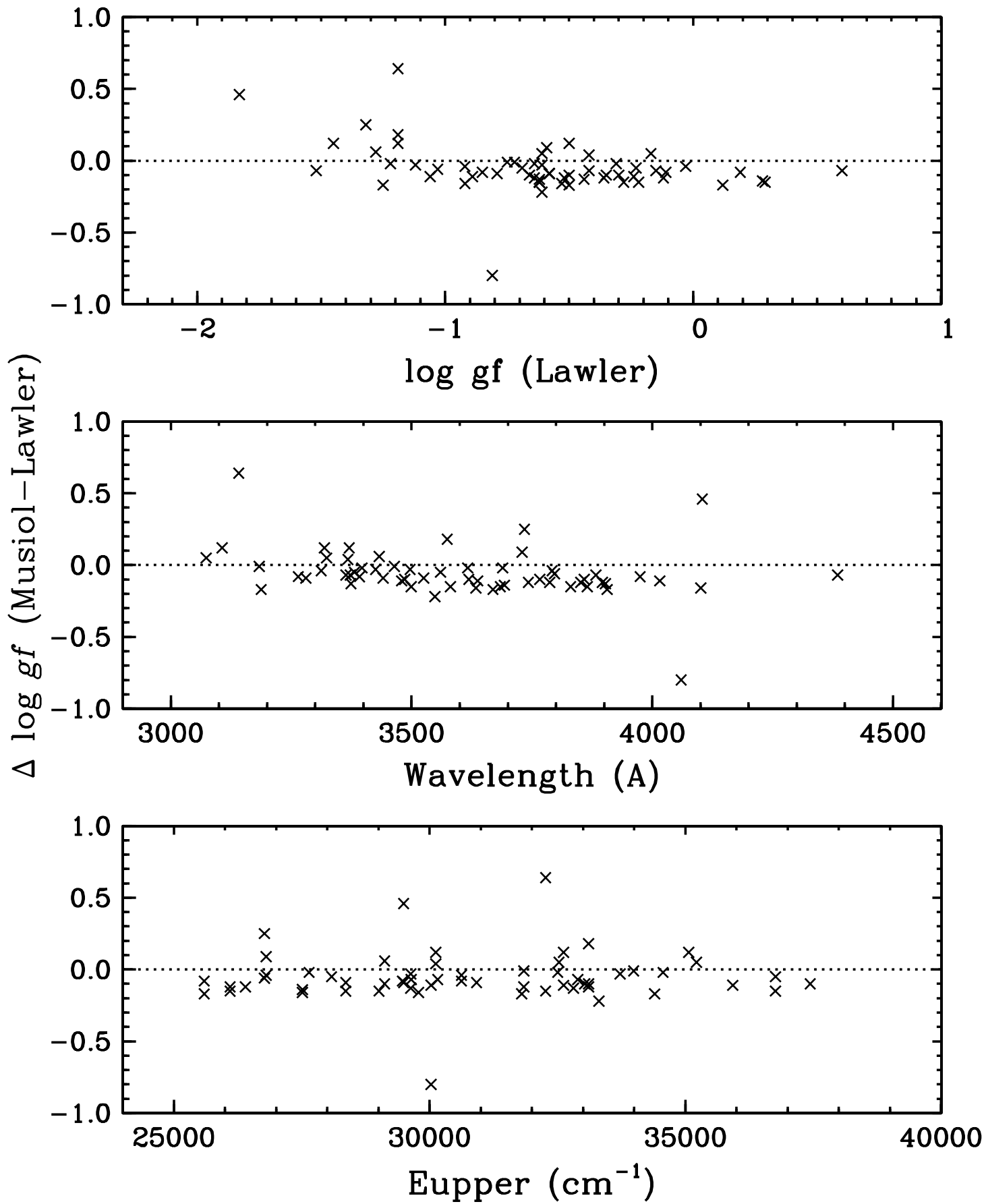
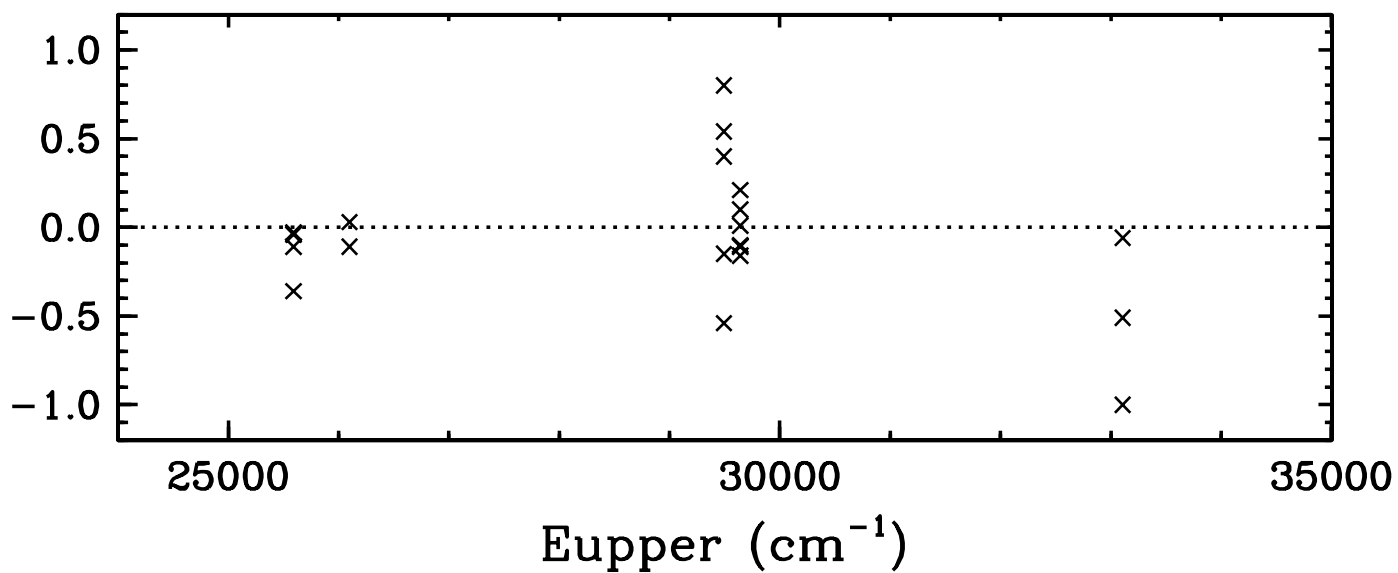
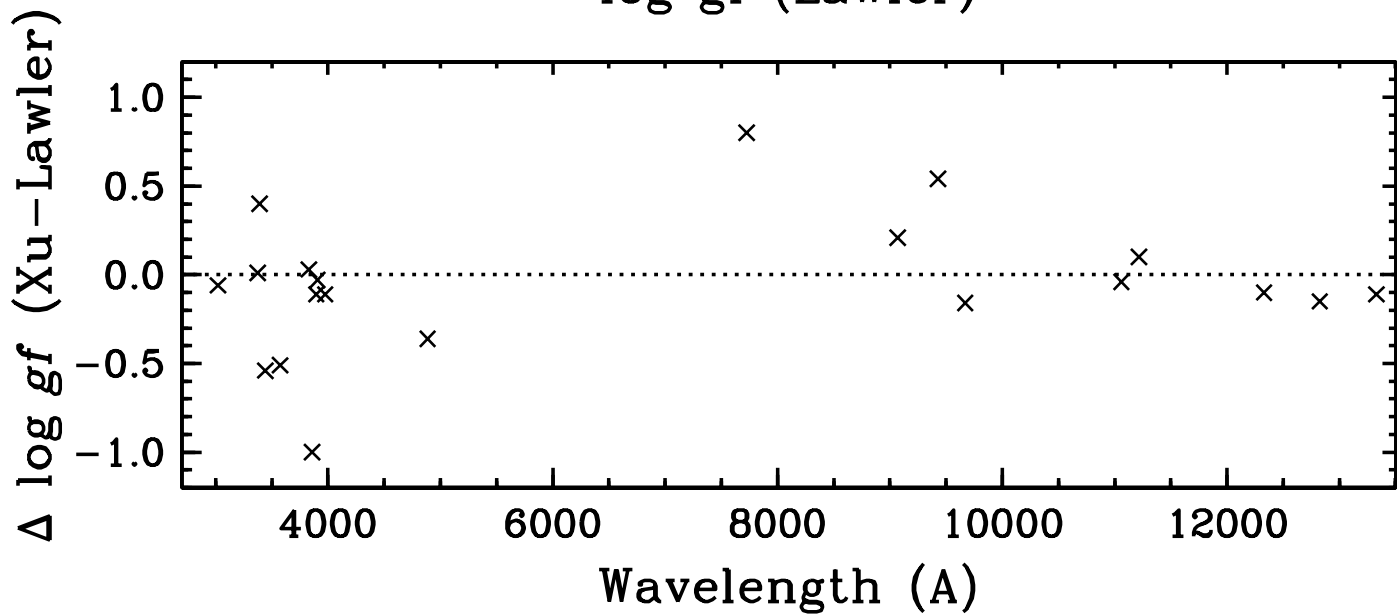
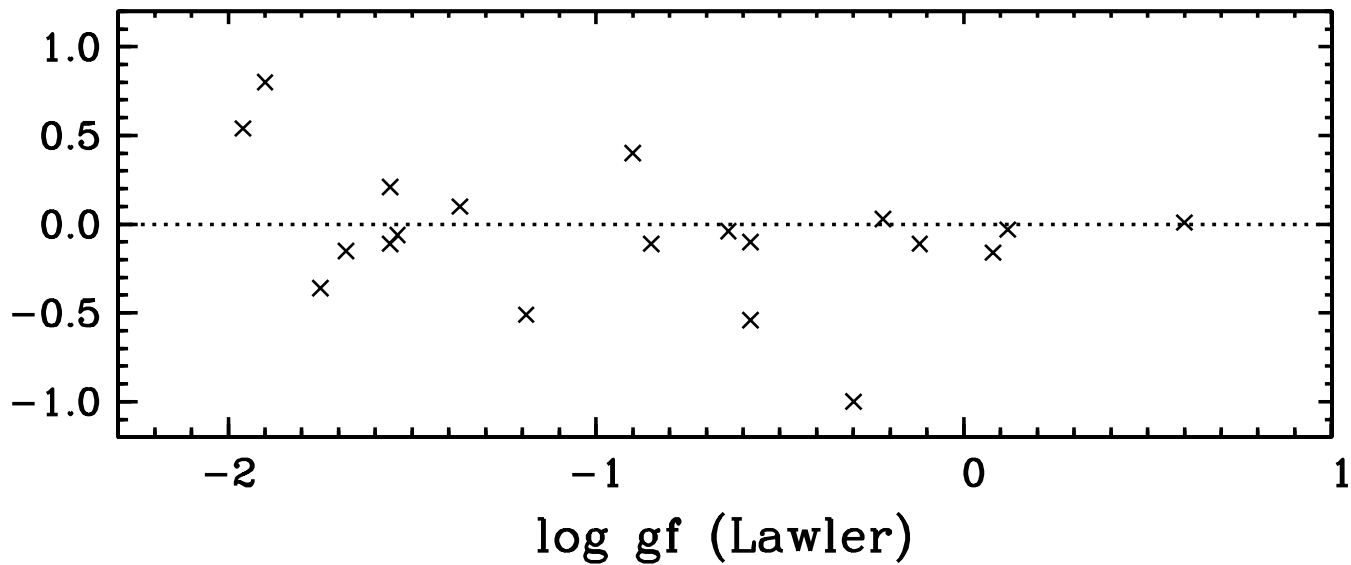


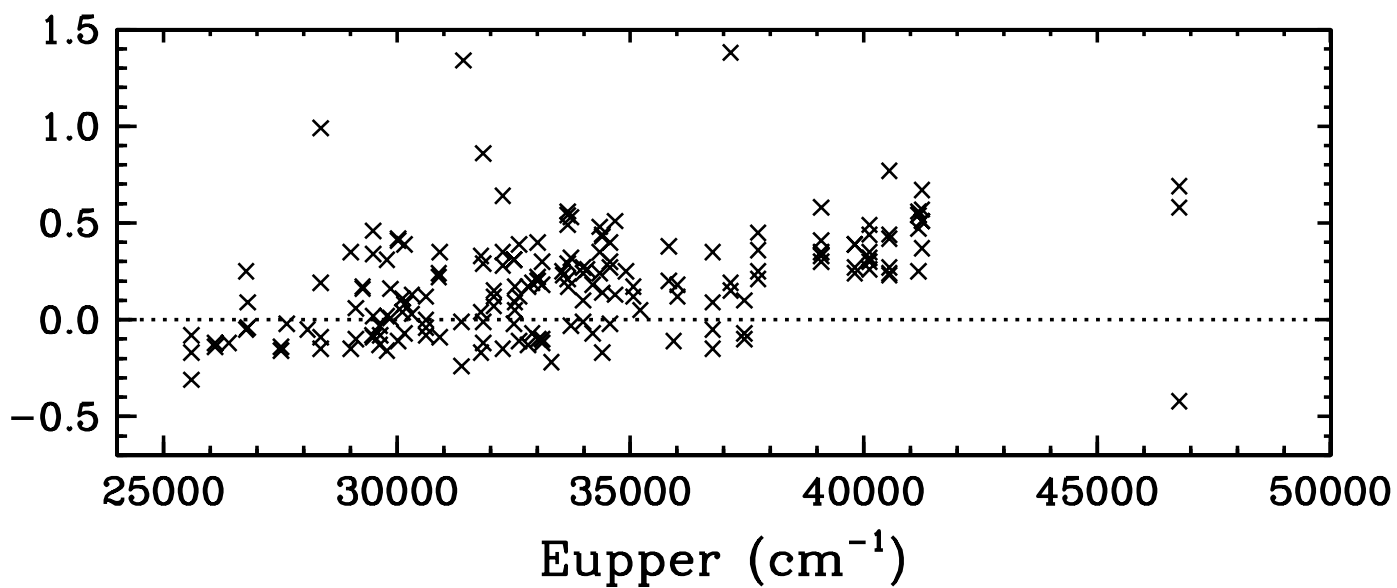
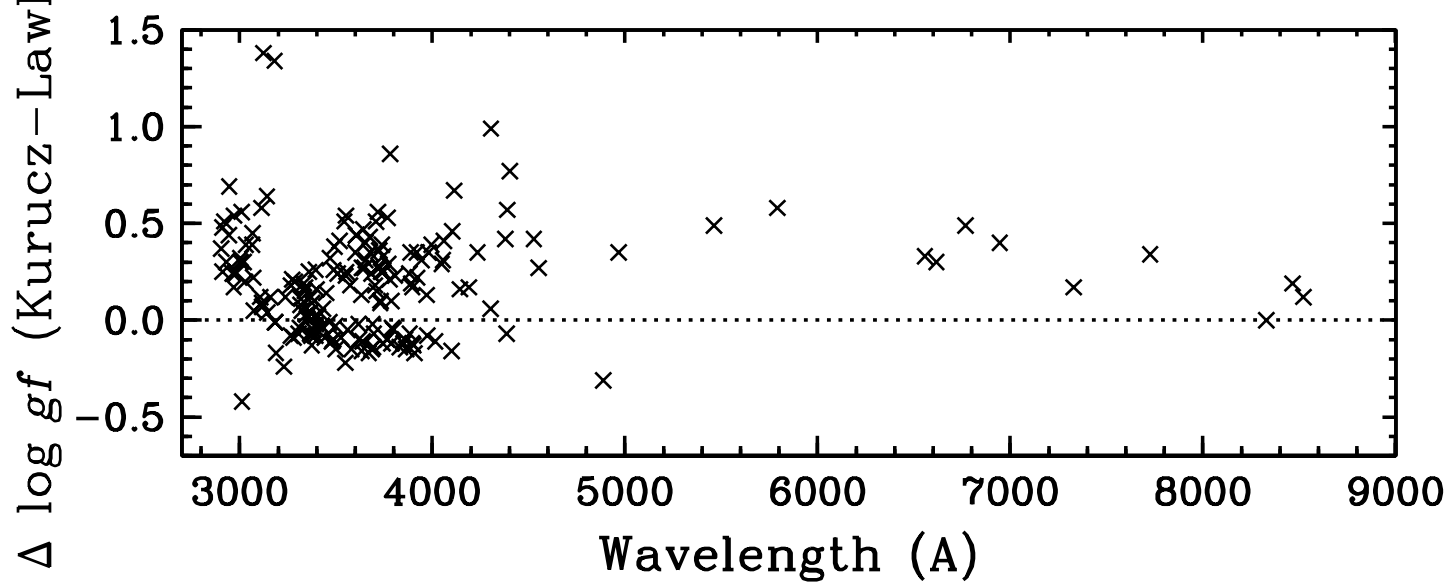
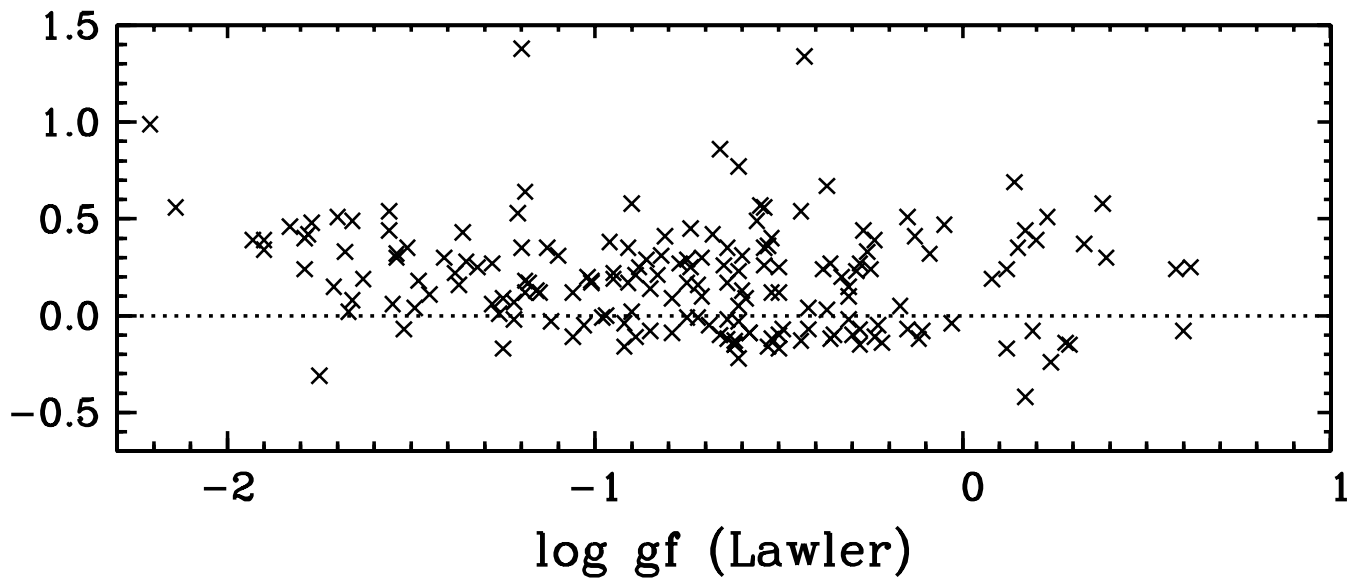
Table 4: Erbium abundances from individual lines in the Sun and the r-process rich metal-poor giant stars.

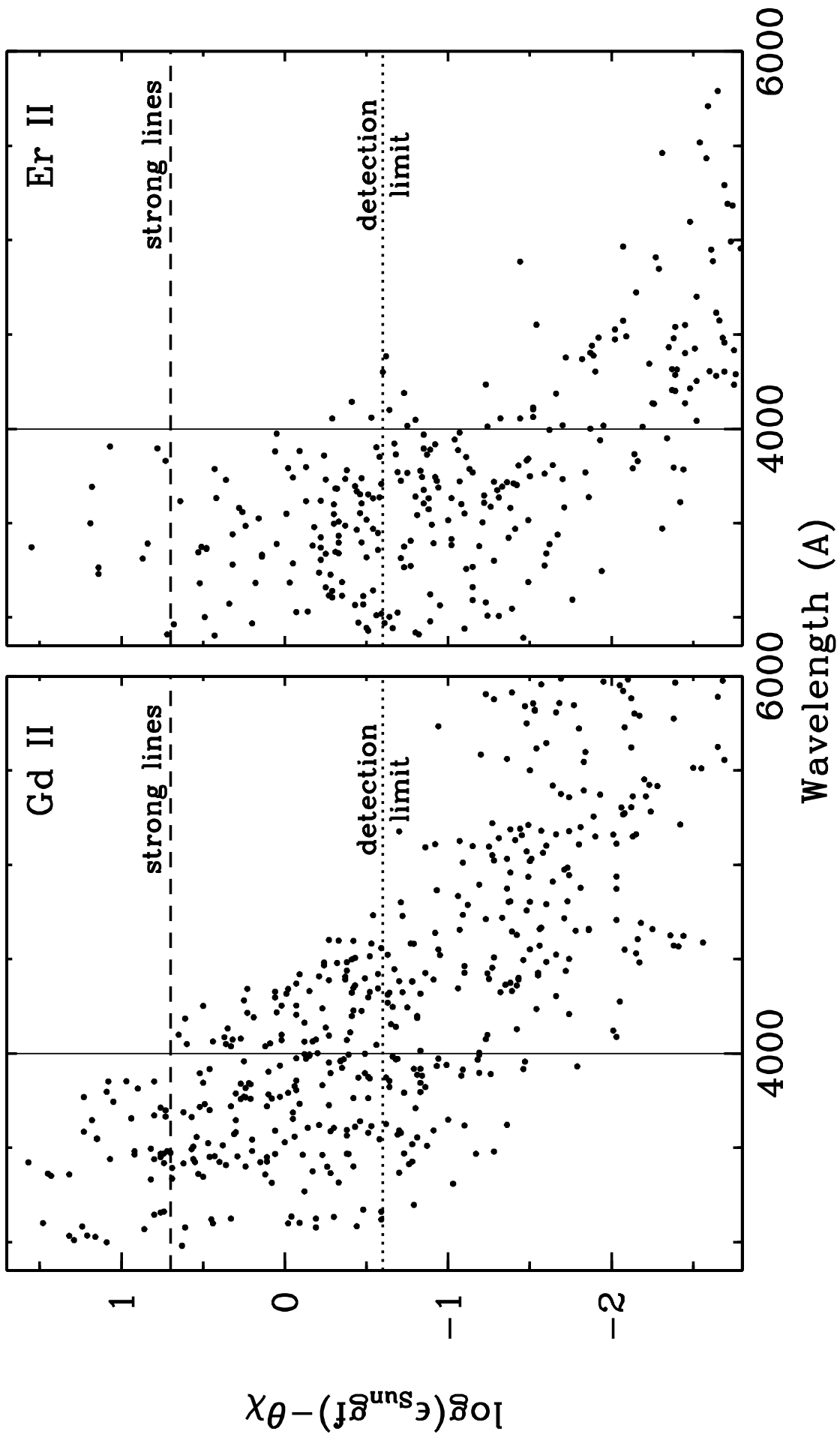
λ (Å)	E. P. (eV)	log(gf)	log ϵ Sun	log ϵ CS 22892	log ϵ BD +17°3248	log ϵ HD 221170	log ϵ HD 115444	log ϵ CS 31082	log ϵ CS 29497	Comment
3230.58	0.055	0.24	0.98	-0.49	? -0.36		-1.26	-0.32	0.59	Cont. unc.
3312.42	0.055	-0.03		-0.47	? -0.23		-1.21	-0.27	0.64	? Messy; Sm II bl.
3332.70	0.886	0.07	0.90	? -0.48	?			-0.29		Messy small bl.
3346.02	0.055	-0.37		-0.42	? -0.24	-0.33	-1.33	?		
3364.07	0.055	-0.42	1.01	-0.52				-0.34		
3499.11	0.055	0.29		-0.52	-0.29	-0.48	-1.28	-0.34	0.47	Ti I, v. wk. in rstars
3559.89	0.000	-0.69		-0.41	-0.23	-0.48	-1.17	-0.30		
3580.52	0.055	-0.62		-0.50	-0.25	-0.48	-1.24	? -0.32		
3616.57	0.000	-0.31		-0.48	-0.26	-0.46	-1.18	? -0.32		Fe I, v. wk. in rstars
3616.62	0.055	-1.03							0.54	? Bl. with 3616.566

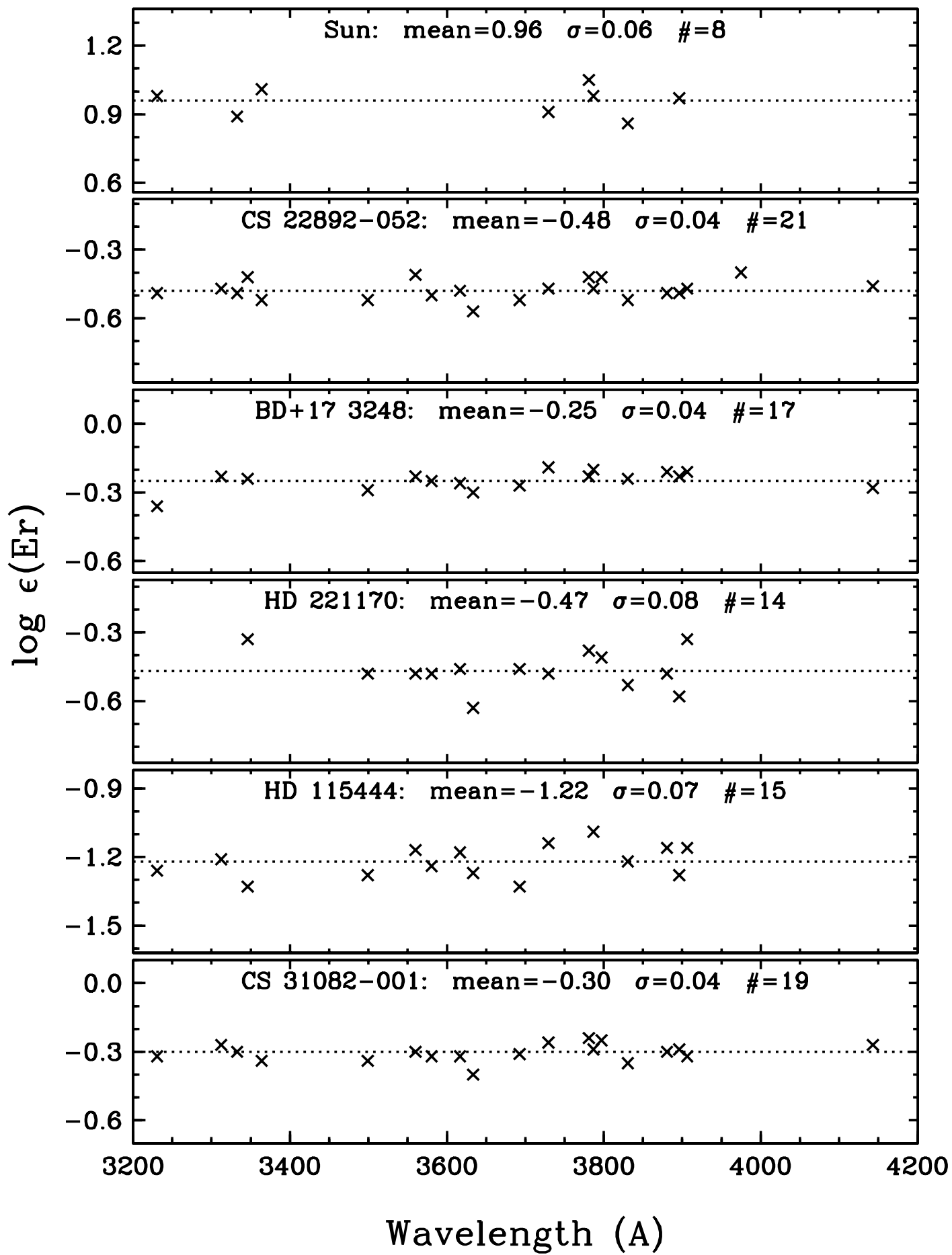
3633.54	0.000	-0.53		-0.57	-0.30	-0.63	-1.27	-0.40		
3692.65	0.055	0.28		-0.52	-0.27	-0.46	-1.33	-0.31	0.49	Fe I, v. wk. in rstars
3729.53	0.000	-0.59	0.91	-0.47	-0.19	-0.48	-1.14	-0.26		
3781.02	0.669	-0.66	1.05	-0.42	-0.23	?	-0.38	-0.24		
3786.84	0.000	-0.52	0.98	-0.47	-0.20		-1.09	? -0.29	0.59	Blending in wings (sun)
3797.06	0.055	-1.03		-0.42		-0.41		-0.25		
3830.48	0.000	-0.22	0.86	-0.52	-0.24	-0.53	-1.22	-0.35	0.64	
3880.61	0.636	-0.25		-0.49	-0.21	-0.48	-1.16	? -0.30		
3896.23	0.055	-0.12	0.97	-0.49	-0.23	-0.58	-1.28	-0.29	0.52	Nd II, wk. in blue wing
3906.31	0.000	0.12		-0.47	-0.21	-0.33	? -1.16	-0.32	0.64	Co I, v. wk. in rstars
3974.72	0.055	-0.85		-0.40						Co I, v. wk. in rstars
4142.91	0.636	-0.72		-0.46	-0.28	?		-0.27		
Er:										
mean			0.96	-0.48	-0.25	-0.47	-1.22	-0.30	0.57	

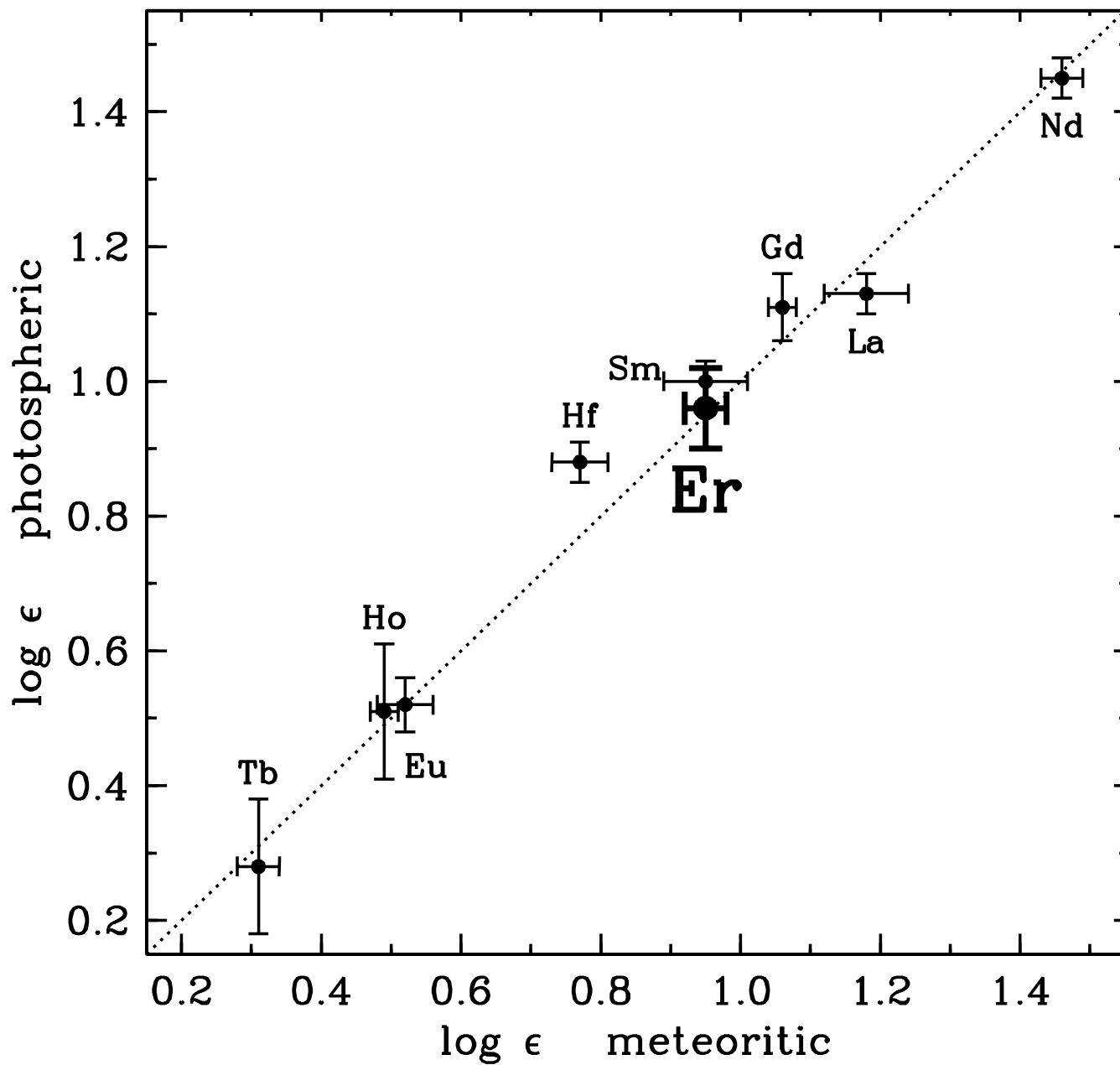
Er: error	0.02	0.01	0.01	0.02	0.02	0.01	0.02
Er: σ	0.06	0.04	0.04	0.08	0.07	0.04	0.07
Er:							
number	8	21	17	14	15	19	9
of lines							
Er:							
median	0.98	-0.48	-0.24	-0.48	-1.22	-0.30	0.59
Eu:							
mean	0.52	-0.95	-0.67	-0.86	-1.63	-0.72	-0.07
Eu-Er	-0.44	-0.47	-0.42	-0.40	-0.41	-0.42	-0.64
Eu-Er solar-r	-0.37						











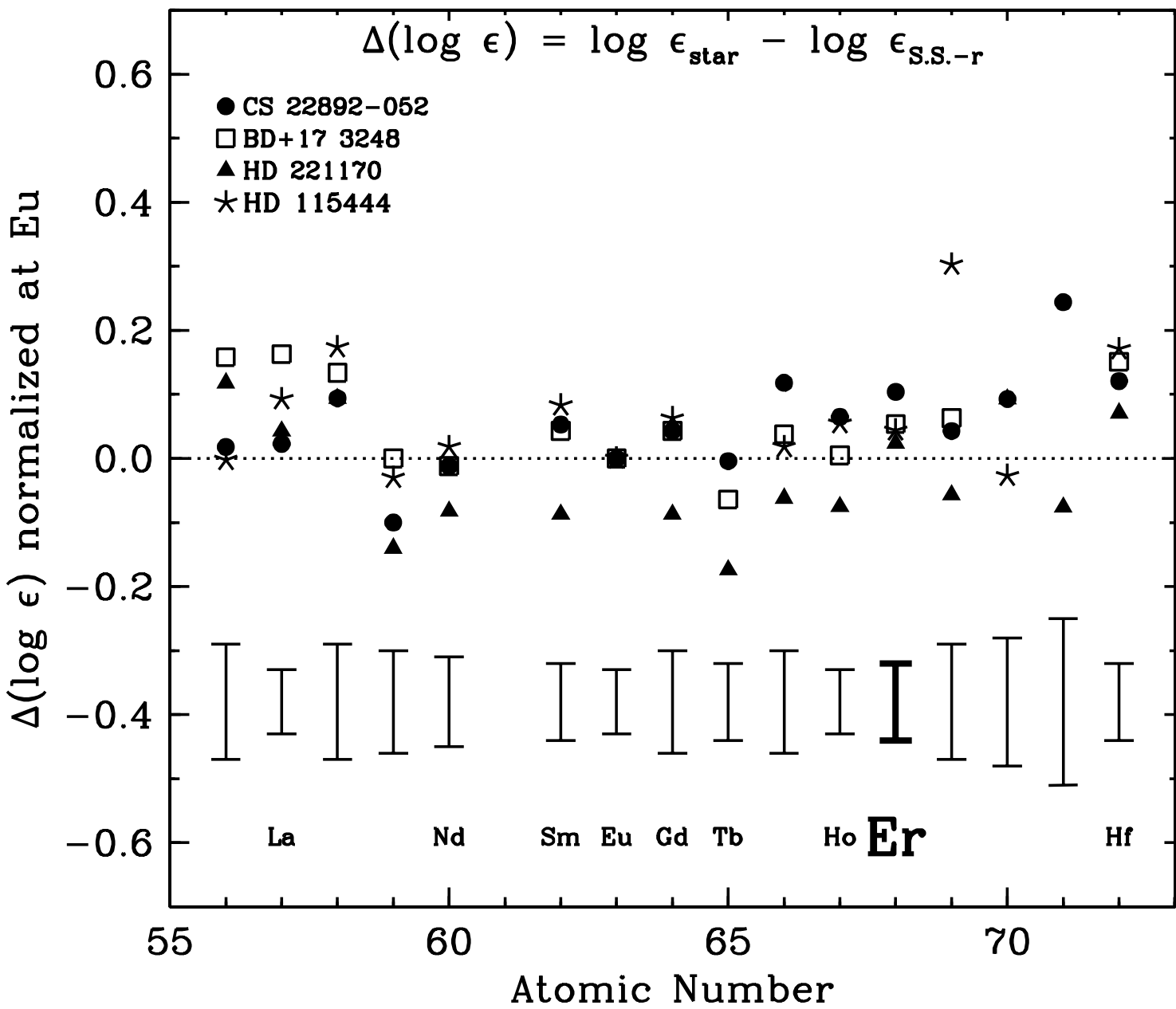


Table 1. Fourier transform spectra of Er lamps used in this study. All were recorded using the 1.0 meter FTS on the McMath telescope at the National Solar Observatory, Kitt Peak, AZ.

Index	Date	Serial Number	Lamp Type ¹	Buffer Gas	Lamp Current (mA)	Wavenumber Range (cm ⁻¹)	Limit of Resolution (cm ⁻¹)	Coadds	Beam Splitter	Filter	Detector ²	Calibration ³
1	1988 Nov. 10	3	Custom HCD	Ar	500	7346 – 42640	0.055	8	UV		S. B. Si Diode	Ar I & II W Strip Lamp
2	1988 Nov. 11	4	Custom HCD	Ar	500	13437 – 42640	0.055	8	UV	CuSO ₄	S. B. Si Diode	Ar I & II W Strip Lamp
3	1987 Jan. 13	2	Custom HCD	Ar	500	8218 – 26091	0.050	8	Vis		S. B. Si Diode	Ar I & II W Strip Lamp
4	1987 Jan. 13	1	Custom HCD	Ar	500	8218 – 26091	0.100	12	Vis		S. B. Si Diode	Ar I & II W Strip Lamp

5	1987 Jan. 14	8	Custom HCD	Ar	300	8218 – 26091	0.050	1	Vis	S. B. Si Diode	Ar I & II W Strip Lamp
6	1987 Jan. 13	5	Custom HCD	Ar	500	3488 – 15077	0.029	8	Vis	InSb	Ar I & II W Strip Lamp
7	2000 Feb. 28	32	Commercial HCD	Ar	26.5	7929 – 34998	0.053	59	UV	S. B. Si Diode	Ar I & II
8	2002 Feb. 26	10	Commercial HCD	Ar	27	7929 – 34998	0.050	50	UV	S. B. Si Diode	Ar I & II WQH Lamp
9	2000 Feb. 28	27	Commercial HCD	Ar	26.5	7929 – 34998	0.053	16	UV	S. B. Si Diode	Ar I & II
10	2000 Feb. 28	26	Commercial HCD	Ar	23	7929 – 34998	0.053	4	UV	S. B. Si Diode	Ar I & II
11	2000 Feb. 28	28	Commercial HCD	Ar	17	7929 – 34998	0.053	4	UV	S. B. Si Diode	Ar I & II
12	1988 Nov. 10	1	Custom HCD	Ne	300	7346 – 42640	0.055	8	UV	S. B. Si	W Strip Lamp

											Diode
13	1988 Nov. 10	2	Custom HCD	Ne	300	13437 – 42640	0.055	8	UV	S. B. Si	W Strip Lamp
											Diode
14	1987 Jan. 13	3	Custom HCD	Ne	300	8218 – 26091	0.050	8	Vis	S. B. Si	W Strip Lamp
											Diode
15	1987 Jan. 13	4	Custom HCD	Ne	310	3488 – 15017	0.029	8	UV	InSb	W Strip Lamp

¹Lamp types include commercially available small sealed Hollow Cathode Discharge (HCD) lamps typically used in atomic absorption spectrophotometers and a custom water-cooled HCD lamp.

²Detectors types include the Super Blue (S. B.) Si photodiode.

³Relative radiometric calibrations were based on selected sets of Ar I and Ar II lines, on a Tungsten-Quartz-Halogen (WQH) lamp calibrated as a secondary irradiance standard, and on a Tungsten (W) Strip Lamp calibrated as a secondary radiance standard.